Cell Reports

Article

TAFA4 relieves injury-induced mechanical hypersensitivity through LDL receptors and modulation of spinal A-type K^+ current

Graphical abstract

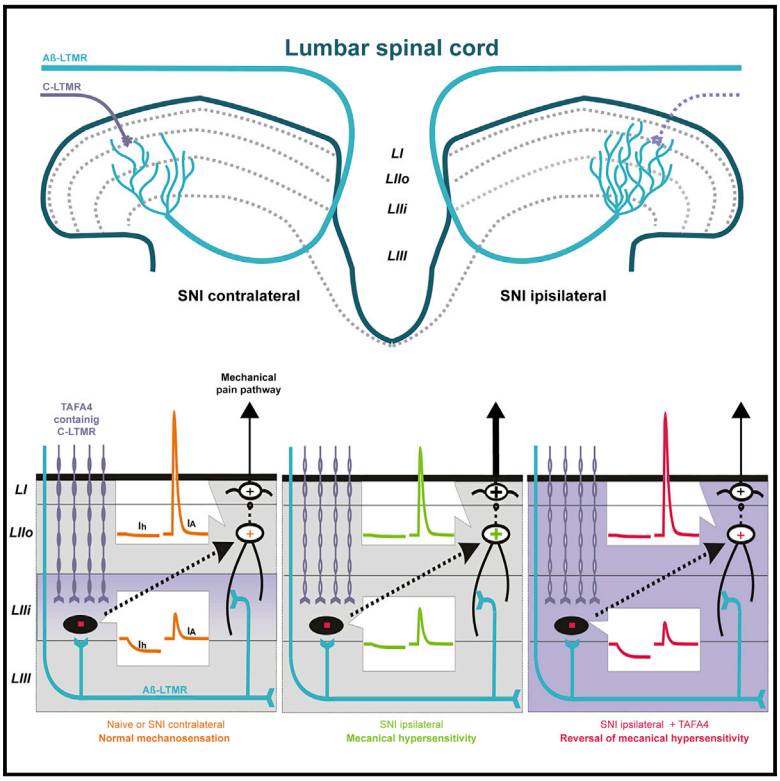

Authors

Sungjae Yoo, Catarina Santos, Ana Reynders, ..., Francis Castets, Nadine Clerc, Aziz Moqrich

Correspondence

francis.castets@univ-amu.fr (F.C.), nadine.clerc@univ-amu.fr (N.C.), aziz.moqrich@univ-amu.fr (A.M.)

In brief

Yoo et al. demonstrate that intrathecal or systemic administration of human recombinant TAFA4 reverses inflammatory, postoperative, and nerve injury-induced mechanical pain. The TAFA4 antihypersensitive effect requires functional RAP-sensitive LDL receptors to restore normal mechanical sensitivity by rescuing the injury-induced alterations of I_A in two distinct subsets of spinal cord dorsal horn interneurons.

Highlights

- TAFA4 reverses inflammatory, postoperative, and nerve injury-induced mechanical pain
- TAFA4-mediated antihypersensitive effect requires functional LDL receptor family members
- SNI alters spinal I_A in opposite direction in excitatory and inhibitory interneurons
- TAFA4 reverses SNI-induced alteration of I_A in both interneuron subtypes

Yoo et al., 2021, Cell Reports *37*, 109884
October 26, 2021
https://doi.org/10.1016/j.celrep.2021.109884

CellPress

Cell Reports

CellPress
OPEN ACCESS

Article

TAFA4 relieves injury-induced mechanical hypersensitivity through LDL receptors and modulation of spinal A-type K^+ current

Sungjae Yoo,[1,8] Catarina Santos,[1,8] Ana Reynders,[1] Irène Marics,[1] Pascale Malapert,[1] Stéphane Gaillard,[2] Aude Charron,[1] Sophie Ugolini,[3] Rafaelle Rossignol,[3] Abderazzak El Khallouqi,[4] Jean-Yves Springael,[5] Marc Parmentier,[5] Andrew J. Saurin,[1] Jean-Marc Goaillard,[6,7] Francis Castets,[1,*] Nadine Clerc,[1,*] and Aziz Moqrich[1,9,*]

[1]Aix-Marseille Université, CNRS, Institut de Biologie du Développement de Marseille, UMR 7288, Case 907, 13288 Marseille Cedex 09, France

[2]Phenotype Expertise, 5 Boulevard du Maréchal Koenig, 13009 Marseille, France

[3]Aix-Marseille Université, CNRS, INSERM, CIML, Centre d'Immunologie de Marseille-Luminy, Marseille, France

[4]RG Functional Neurobiology, Institute for Developmental Biology and Neurobiology, Johannes Gutenberg University Mainz, Mainz 55128, Germany

[5]Institut de Recherche Interdisciplinaire en Biologie Humaine et Moléculaire, Université Libre de Bruxelles, Campus Erasme, 808 Route de Lennik, 1070 Bruxelles, Belgique

[6]UMR_S 1072, Aix-Marseille Université, INSERM, Faculté de Médecine Secteur Nord, Marseille, France

[7]Present address: INT, Aix Marseille Université, CNRS, Campus Santé Timone, Marseille, France

[8]These authors contributed equally

[9]Lead contact

*Correspondence: francis.castets@univ-amu.fr (F.C.), nadine.clerc@univ-amu.fr (N.C.), aziz.moqrich@univ-amu.fr (A.M.)

https://doi.org/10.1016/j.celrep.2021.109884

SUMMARY

Pain, whether acute or persistent, is a serious medical problem worldwide. However, its management remains unsatisfactory, and new analgesic molecules are required. We show here that TAFA4 reverses inflammatory, postoperative, and spared nerve injury (SNI)-induced mechanical hypersensitivity in male and female mice. TAFA4 requires functional low-density lipoprotein receptor-related proteins (LRPs) because their inhibition by RAP (receptor-associated protein) dose-dependently abolishes its antihypersensitive actions. SNI selectively decreases A-type K^+ current (I_A) in spinal lamina II outer excitatory interneurons (L-IIo ExINs) and induces a concomitant increase in I_A and decrease in hyperpolarization-activated current (I_h) in lamina II inner inhibitory interneurons (L-IIi InhINs). Remarkably, SNI-induced ion current alterations in both IN subtypes were rescued by TAFA4 in an LRP-dependent manner. We provide insights into the mechanism by which TAFA4 reverses injury-induced mechanical hypersensitivity by restoring normal spinal neuron activity and highlight the considerable potential of TAFA4 as a treatment for injury-induced mechanical pain.

INTRODUCTION

Pain is commonly classified as acute or chronic. Acute pain is short lived and essential for maintenance of our physical integrity, whereas chronic pain persists beyond the normal time of healing and adversely affects our well-being. Chronic inflammatory, neuropathic, or postoperative pain gives rise to long-lasting sensory abnormalities, such as hyperalgesia (extreme pain evoked by noxious stimuli) and mechanical allodynia (pain evoked by innocuous mechanical stimuli). These categories of pain differ in terms of etiology and clinical features, but they have several mechanisms in common, including alterations of neuro-immune interactions and neuron sensitization peripherally and centrally (Costigan et al., 2009). There is growing evidence to suggest that loss of inhibition may be a key mechanism underlying chronic pain (Bourane et al., 2015a, 2015b; Boyle et al., 2019; Coull et al., 2005; Duan et al., 2014; Peirs et al., 2015; Petitjean et al., 2015, 2019; Zeilhofer et al., 2012; Zhang et al., 2018). However, despite our extensive knowledge of the mechanisms and circuits underlying chronic pain in rodents, translation of these findings into effective treatments for chronic pain in humans remains unsatisfactory (Colloca et al., 2017). Indeed, non-steroidal anti-inflammatory drugs (NSAIDs) have limited efficacy against chronic pain, and opioids have multiple adverse effects, including potentially lethal respiratory depression, nausea, constipation, hyperalgesia, tolerance, and physical and psychological dependence (Benyamin et al., 2008). Thus, efforts to identify new targets with analgesic potential for treatment of chronic pain should be encouraged.

In the last few years, we have discovered striking features of the secreted protein TAFA4, suggesting that it might be an ideal drug for treatment of chronic pain. TAFA4 belongs to a family of five highly conserved secreted neurokines with a striking degree of amino acid identity among orthologs from divergent species

(Sarver et al., 2021). TAFA4 contains a signal peptide followed by a highly conserved core region with 10 cysteine residues, including a CC-chemokine motif, that make it resemble a cytokine (Tom Tang et al., 2004). In contrast to the other members of the FAM19A family, TAFA4 is highly enriched in the peripheral nervous system with preferential expression in C-low-threshold mechanoreceptors (C-LTMRs), which are known to express vesicular glutamate transporter type 3 (VGLUT3) and tyrosine hydroxylase (TH) (Li et al., 2011; Seal et al., 2009). C-LTMRs project onto the innermost layer of lamina II (L-II) in the dorsal horn of the spinal cord (DHSC), in which the innocuous mechanoreceptive and nociceptive pathways overlap.

We have shown that, in mice in which the TAFA4 gene is deleted, mechanical hypersensitivity induced by nerve injury lasts much longer than in wild-type (WT) mice (Delfini et al., 2013). These phenotypes are reversed by intrathecal injection of recombinant TAFA4. Furthermore, TAFA4 increases the frequency of spontaneous inhibitory postsynaptic currents in L-II DHSC interneurons, suggesting enhancement of spinal inhibitory tone (Kambrun et al., 2018). Consistent with our results for animal models, human psychophysical studies have shown that, in addition to their crucial role in pleasant touch sensation, C-LTMRs are also involved in pain modulation (Ackerley et al., 2014; Löken et al., 2009; McGlone et al., 2014; Olausson et al., 2002). Thus, manipulation of the activity of C-LTMRs or of their biological content is a potentially powerful strategy for treatment of chronic pain.

Here we report experimental evidence demonstrating that TAFA4 possesses powerful actions against pathologically increased mechanical pain. We first show that, in male and female mice, intrathecal and subcutaneous administration of human recombinant TAFA4 reverses inflammatory, postoperative, and nerve injury-induced mechanical hypersensitivity. We then demonstrate that TAFA4 action requires functional members of low-density lipoprotein receptor-related proteins (LRPs) because inhibition of these receptors by RAP *in vivo* abolished its antihypersensitive action in the postoperative and neuropathic pain models. We also show that TAFA4 can reverse nerve injury-induced neuronal sensitization of the spinal L-II interneurons reported to be responsible for mechanical threshold alterations. We chose to focus on A-type K^+ currents (I_A) because they are known to play a critical role in spinal cord pain processes (Hu et al., 2006), and we also suspected their levels to be low in L-II neurons of TAFA4-null mice (Delfini et al., 2013). We found that spared nerve injury (SNI) provoked profound differential alterations to I_A in L-II inhibitory and excitatory interneurons, which were reversed by recombinant TAFA4 in an LRP-dependent manner.

RESULTS

TAFA4 reverses injury-induced mechanical hypersensitivity in various pain models

In two previous studies (Delfini et al., 2013; Kambrun et al., 2018), we showed that intrathecal (IT) injection of TAFA4 reversed carrageenan- and complete Freund's adjuvant (CFA)-induced mechanical hypersensitivity in male mice. We further explored the potential of TAFA4 as an analgesic molecule by extending our investigation to other preclinical pain models in male and female mice using IT and systemic subcutaneous (s.c.) injections. We used SNI as a model of neuropathic pain, paw incision as a model of postoperative pain, and intraplantar paw injection of carrageenan as a model of inflammatory pain. In the SNI model, recombinant TAFA4 (170 pmol injected IT or 300 μg/kg injected s.c.) provided significant reversal of mechanical hypersensitivity, as shown by a significant increase in mechanical thresholds for up to 4 h after injection (Figures 1A, 1B, S1A, and S1B). The optimal concentration of TAFA4 for s.c. administration was determined after injection of three different doses: 12, 60, and 300 μg/kg (Figure S1C). S.c. injection of 300 μg/kg TAFA4 provided significant reversal of mechanical hypersensitivity in male and female mice in the SNI model. Furthermore, injection of 300 μg/kg of TAFA4 to naive of SNI mice affected neither the locomotor activity nor the anxiety levels of the mice (Figure S1D). We therefore used this concentration for the paw incision and carrageenan-induced inflammation models. In both paradigms, on days 1 and 2 after injury, male and female mice displayed mechanical hypersensitivity, and IT injection of 170 pmol or s.c. administration of 300 μg/kg TAFA4 provided significant reversal of mechanical hypersensitivity for up to 4 h after administration (Figures 1C–1F). In all three pain models, IT or s.c. administration of TAFA4 had no effect on the mechanical thresholds of the contralateral paws (Figures 1A–1F). Consistent with these findings, IT injection of morphine had a significant analgesic effect in response to infrared heat stimulation, but IT administration of recombinant TAFA4 or BSA had no effect on the heat threshold of the mouse's tail (Figure S1E). Finally, using the SNI model, we compared the effect of TAFA4 with those of SNC-80 (an agonist of the delta opioid receptor), DAMGO (an agonist of the μ opioid receptor), and baclofen (an agonist of the $GABA_B$ receptor). We found that IT injection of TAFA4 induced a reversal of SNI-induced mechanical hypersensitivity that was of a similar magnitude to that induced by SNC80, DAMGO, or baclofen but lasted significantly longer (Figure S1F). Overall, these results demonstrate that TAFA4 does not exert general antinociceptive actions in non-injured animals but strongly reverses mechanical hypersensitivity caused by nerve injury, surgery, and inflammatory agents in male and female mice.

TAFA4 reverses injury-induced mechanical hypersensitivity through RAP-sensitive members of LRPs

It has been suggested that TAFA4 mediates its biological effects through the formyl peptide receptor1 (FPR1) (Wang et al., 2015). We therefore investigated whether N-formyl-Met-Leu-Phe (fMLF; an FPR1 agonist) was able to modulate SNI-induced mechanical hypersensitivity in a manner similar to TAFA4. IT injection of 170 pmol TAFA4 triggered a strong reversal of SNI-induced mechanical hypersensitivity, whereas the IT administration of 2.5 pmol or 2.5 nmol fMLF had no effect. Furthermore, co-administration of 2.5 nmol fMLF did not interfere with the effect of TAFA4 (Figure 2A). Moreover, TAFA4 was unable to activate FPR1 in β-arrestin recruitment assays (Figure 2B) or to promote aequorin-based calcium mobilization in cells expressing FRP1, FPR2, FPR3, or a range of chemokine receptors

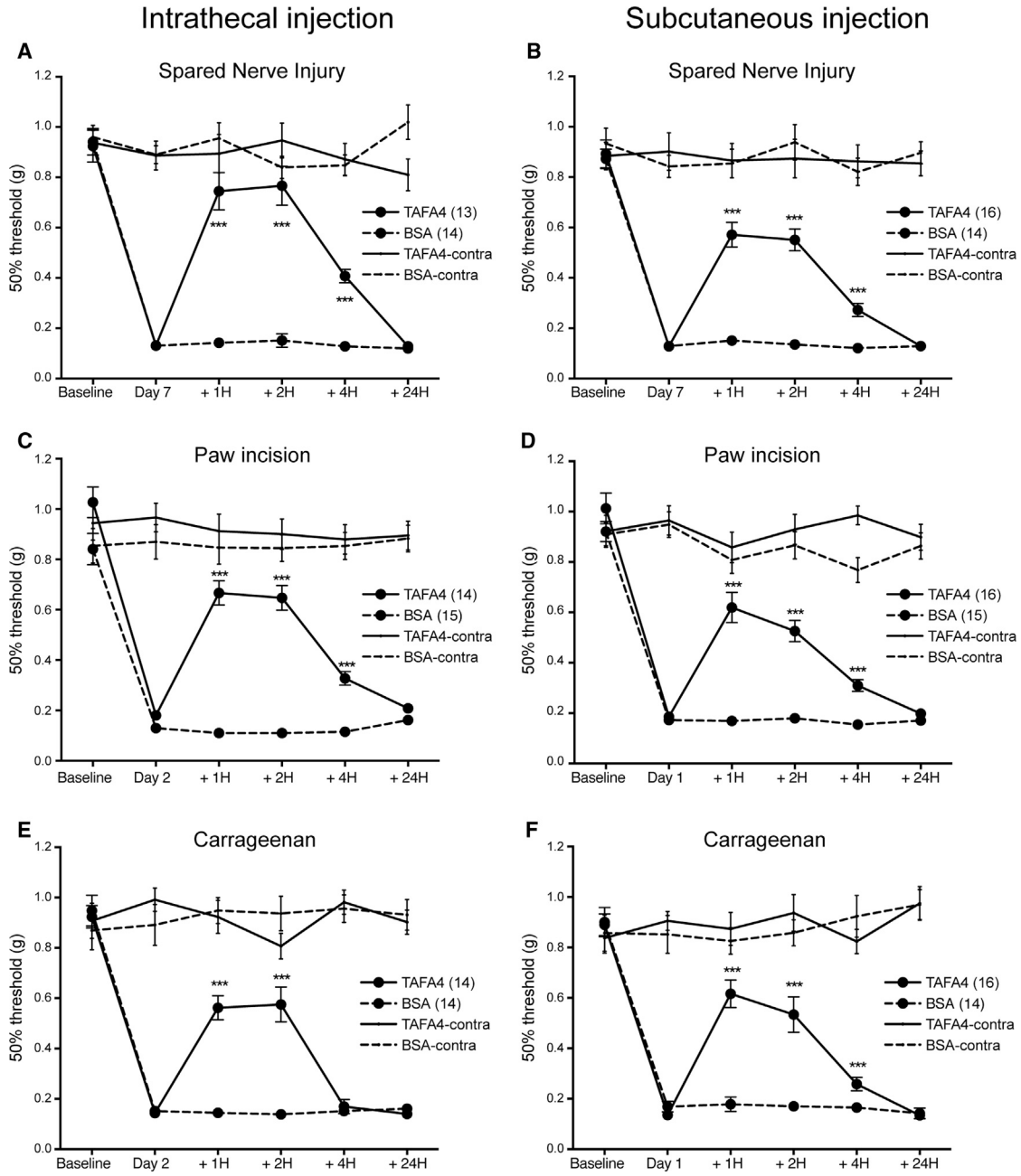

Figure 1. TAFA4 reverses the mechanical hypersensitivity induced by SNI, paw incision, and carrageenan

(A) A significant increase in the threshold for paw withdrawal in response to static mechanical stimulation (von Frey assay) was observed on the ipsilateral but not contralateral (Contra) side of SNI mice receiving IT injections of TAFA4 (n = 13) relative to the control group, which was treated with BSA (n = 14).

(B) TAFA4 also provided significant reversal of mechanical hypersensitivity when administered s.c. to mice undergoing SNI (n = 16). BSA-treated mice remained hypersensitive (n = 14). TAFA4 had no effect on the mechanical thresholds of the Contra paw.

(C and D) IT and s.c. administration of TAFA4 induced a significant increase in the threshold of paw withdrawal in response to static mechanical stimulation following paw incision on the ipsilateral but not Contra side (n = 14 for IT and n = 16 for s.c. administration) relative to the control group treated with BSA (n = 15 for both modes of administration).

(E and F) Carrageenan-induced mechanical hypersensitivity was reversed by IT or s.c. administration of TAFA4 (n = 14 for IT and n = 16 for SC administration) but not by administration of BSA (n = 14 for IT and s.c. administration).

Results are expressed as mean ± SEM. ***$p < 0.001$ for comparisons of TAFA4-treated and BSA-treated mice (multiple t tests). See also Figure S1.

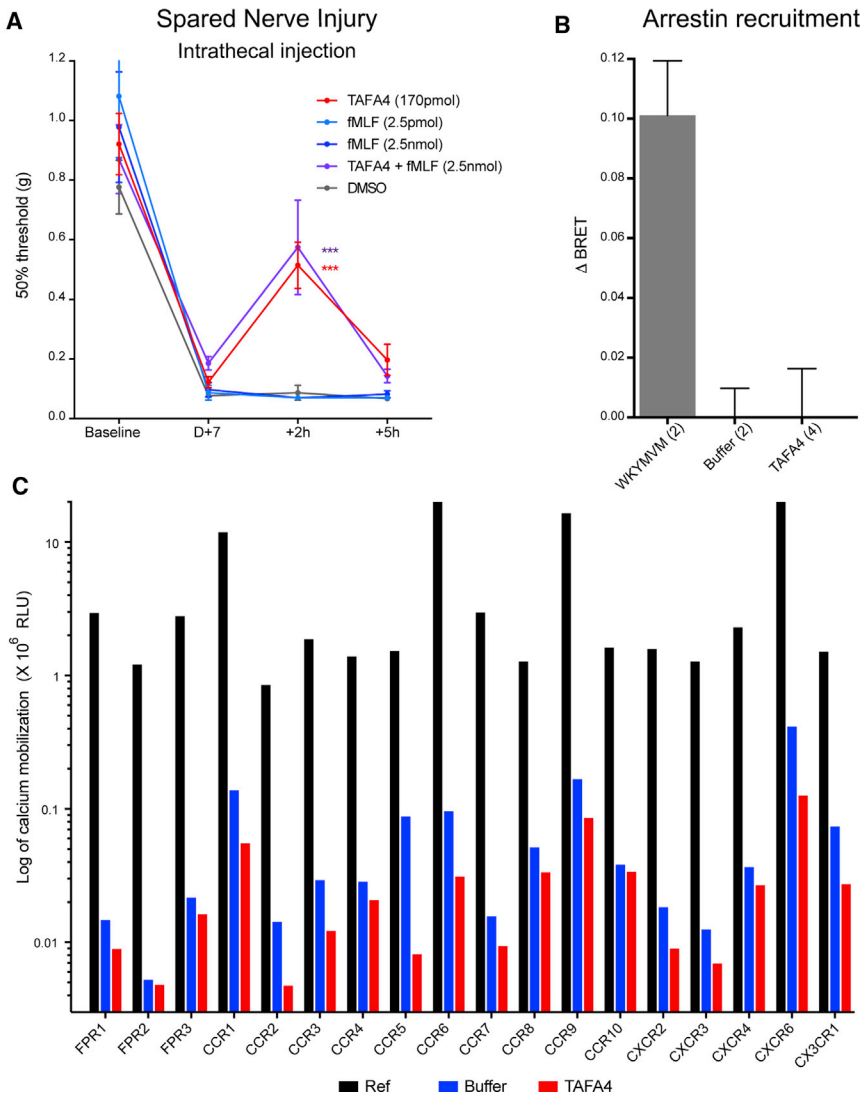

Figure 2. The antihypersensitive action of TAFA4 is mediated neither by FPR1 nor chemokine receptors

(A) The acute anti-hypersensitive effect of IT administration of 170 pmol of TAFA4 alone (red) or 0.25 pmol (light blue) or 250 nmol (dark blue) fMLF alone or in combination with 170 pmol TAFA4 (cyan) on day 7 after SNI. IT injection of DMSO (gray) had no effect on SNI-induced mechanical hypersensitivity. Results are expressed as mean ± SEM. ***$p < 0.001$ versus DMSO-treated mice (multiple t tests).

(B) Real-time measurement of BRET signals in HEK293T cells expressing β-arrestin2-*R*Luc and FPR1-EYFP after stimulation with 100 nM WKYMVM, TAFA4, or dilution buffer. The results are expressed as the difference between BRET signals (ΔBRET) measured in the presence and absence of stimulation. The data shown are the mean ± SEM for 2–4 independent experiments.

(C) Calcium mobilization was measured in Chinese hamster ovary (CHO)-K1 cells stably expressing apoaequorin, $G\alpha_{16}$, and the receptor of interest. Cells were stimulated with 100 nM WKYMVM (FPR1 and FPR2); 1 μM WKYMVM (FPR3); 100 nM of the chemokines CCL1 (CCR8), CCL2 (CCR2), CCL5 (CCR1, CCR3, CCR5), CCL17 (CCR4), CCL19 (CCR7), CCL20 (CCR6), CCL25 (CCR9), CCL27 (CCR10), CXCL2 (CXCR2), CXCL11 (CXCR3), CXCL12 (CXCR4), CXCL16 (CXCR6), and CX3CL1 (CX3CR1); or 100 nM TAFA4; luminescence was recorded for 30 s.

(Figure 2C). Therefore, TAFA4 does not transduce its biological effect through FPR1 or through any of the chemokine and chemokine-like receptors tested.

A study by Khalaj et al. (2020) showed that TAFA1–TAFA4 and neurexins interact with each other by establishing intermolecular disulfide bonds during transport through the secretory pathway. This study demonstrates that TAFA proteins are key regulators of neurexin post-translational modifications but also suggest that TAFA4 proteins cannot be considered as traditional secreted ligands that bind neurexins. Therefore, we sought to identify the TAFA4 receptor. To do so, we performed a yeast two-hybrid (Y2H) assay with the full-length TAFA4 as bait, to screen an adult mouse brain expression library. We tested 94 million interactions in total, and 32 putative protein-protein interactions were identified. Eight of the identified clones encoded the E3 ubiquitin-protein ligase DZIP3, five encoded glutaredoxin-3, and 19 clones encoded parts of the 650-kDa LRP1 (9 clones) and LRP1b (10 clones) (Figure S2A).

We focused on the interaction of TAFA4 with LRP1 (Figure 3A) rather than the other putative partners for two reasons: (1) TAFA4 is a secreted protein and would therefore be able to bind to the large extracellular domain of LRP1 and LRP1b, and (2) literature searches showed that LRP1 played a greater physiological role than LRP1b. Indeed, mice lacking LRP1b are viable and fertile and have no damaging phenotypes (Marschang et al., 2004), whereas loss of LRP1 is embryonic lethal (Herz et al., 1992), and its conditional inactivation in Schwann cells, microglia, or neurons leads to impaired pain sensation as well as neurodegeneration (Brifault et al., 2019; Liu et al., 2010; Orita et al., 2013).

A glutathione S-transferase (GST) pull-down assay was performed to validate the physical interaction between TAFA4 and LRP1. The TAFA4/GST fusion protein was produced in a bacterial system, and secreted forms of domains II, III, and IV of LRP1 fused to the green fluorescent protein (GFP) were expressed in human embryonic kidney 293T (HEK293T) cells. TAFA4 interacted strongly with domain IV, slightly with domain III, and not at all with domain II of LRP1 (Figure 3B). RAP, which is known to interact with and block ligand binding to a wide range of LDL receptors, such as LRP1, LRP1b, LRP2, the very-low-density lipoprotein (VLDL) receptor, and apoE receptor 2 (Lee et al., 2007) was used as a control (Figure 3B). The TAFA4/LRP1

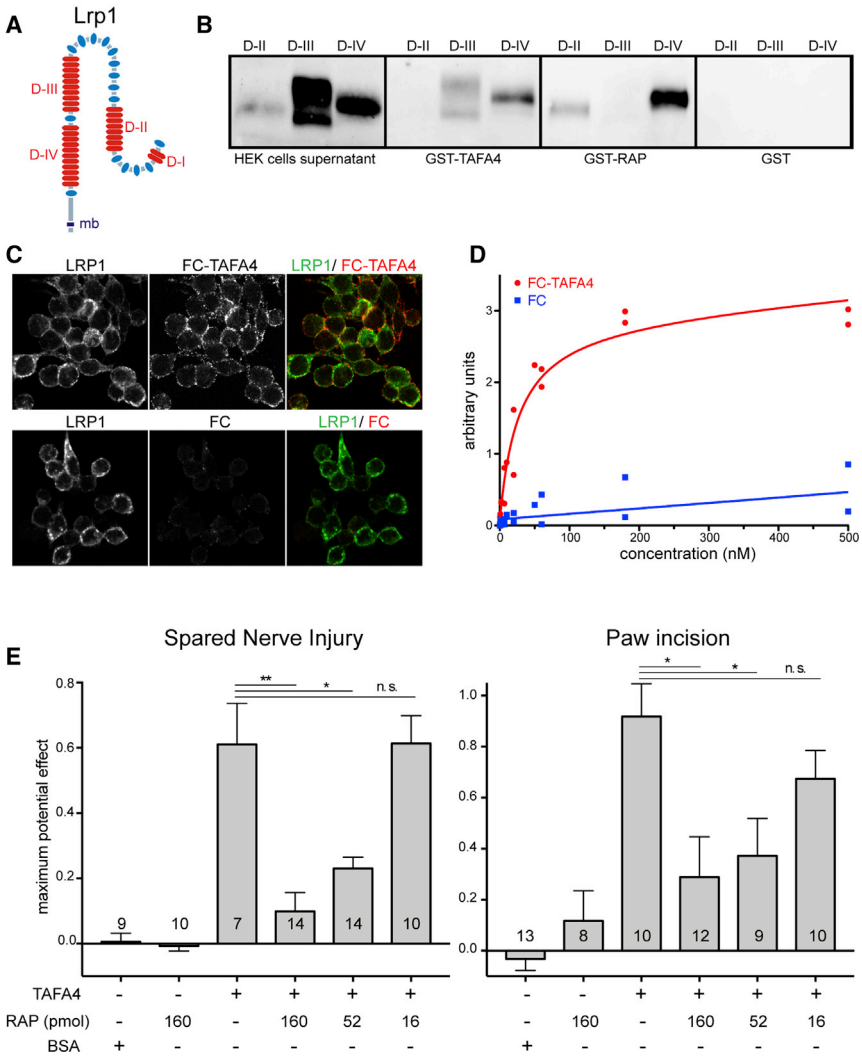

Figure 3. The antihypersensitive action of TAFA4 requires functional RAP-sensitive LRPs

(A) Schematic of the mouse LRP1 proteins, depicting the different subdomains known to engage in protein-protein interactions.

(B) Western blot with anti-GFP antibodies showing that TAFA4 interacts with domains III and IV of LRP1. RAP interacts with domains II and IV. See also Figure S2.

(C) RAW-264.7 cells stained with Fc-TAFA4 or Fc alone or in combination with anti-LRP1 antibody.

(D) Receptor saturation binding assay with RAW-264.7 cells in the presence of various concentrations of Fc-TAFA4 (red curve) or Fc alone (blue curve). The data come from three independent experiments.

(E) Acute anti-hypersensitive effect of IT administration of TAFA4 alone (170 nmol), RAP alone (160 pmol), or TAFA4 in combination with decreasing amounts of RAP on day 7 after SNI (left) and on day 1 following paw incision (right). IT injection of BSA had no effect on injury-induced mechanical hypersensitivity in either of the pain models. The maximum potential effect was calculated as the difference between the withdrawal threshold 2 h after injection and the withdrawal threshold before injection, divided by the difference between the baseline response and the withdrawal threshold before injection. Results are expressed as mean ± SEM for the indicated mouse numbers. $^{**}p < 0.01$, $^{*}p < 0.05$ for comparisons of TAFA4-treated versus TAFA4 + RAP-treated mice (unpaired t tests).

interaction was further confirmed in fluorescence microscopy-based binding and saturation assays on RAW-264.7 cells, which are known to express high levels of LRP1 (Figures 3C and 3D). Finally, for functional confirmation that TAFA4 mediates its biological effects through LRP1, we performed behavioral pharmacology experiments in the SNI and paw incision models. In both paradigms, six cohorts of mice were subjected to injury, and injury-induced mechanical hypersensitivity was confirmed at appropriate time points. The mice in each cohort received an IT injection of 170 pmol recombinant TAFA4 alone, 160 pmol RAP alone, or 170 pmol TAFA4 plus various amounts of RAP (160, 52, or 16 pmol) and BSA. TAFA4 alone provided significant reversal of injury-induced pain hypersensitivity, as shown by the significant increase in mechanical threshold. IT administration of RAP alone had no effect, whereas its co-administration with TAFA4 abolished TAFA4-mediated reversal of mechanical hypersensitivity in a dose-dependent manner (Figure 3E). Given that TAFA4 interacts with at least LRP1 and LRP1b, these data demonstrate that the antihypersensitive effect of TAFA4 requires functional RAP-sensitive LRPs.

TAFA4 reverses the SNI-mediated alterations to spinal I_A and I_h

We showed in a previous study that ablation of the TAFA4 gene causes prolonged injury-induced mechanical hypersensitivity (Delfini et al., 2013). This phenotype was attributed to selective dysregulation of I_A in unidentified L-II interneuron subtypes. In dorsal horn interneurons, I_A, mainly carried by Kv4 channels, is essential for modulation of neuronal excitability and nociceptive behaviors (Hu et al., 2006). This ion current also plays a crucial role in sensitization of L-II outer (L-IIo) excitatory interneurons (ExINs), as shown in a mouse model of capsaicin-induced paw inflammation (Zhang et al., 2018). We therefore investigated whether TAFA4 could reverse I_A alterations reflecting dorsal horn IN sensitization in a preclinical model of neuropathic pain. We chose to use the SNI model because accurate mapping of the spinal segment from which INs are selected for patch-clamp recording is possible in this model. Indeed, SNI induces massive microglial activation that can be visualized as fluorescently labeled IB4 in living tissue within the spinal segments in which axotomized afferents terminate (Boscia et al., 2013).

We used this approach and lumbar spinal cord slices from WT mice that were naive or subjected to SNI to screen a large number of INs by blind voltage-clamp recordings in L-IIo and L-II inner (L-IIi; Figure 4A). The classic voltage-step protocol (Figures

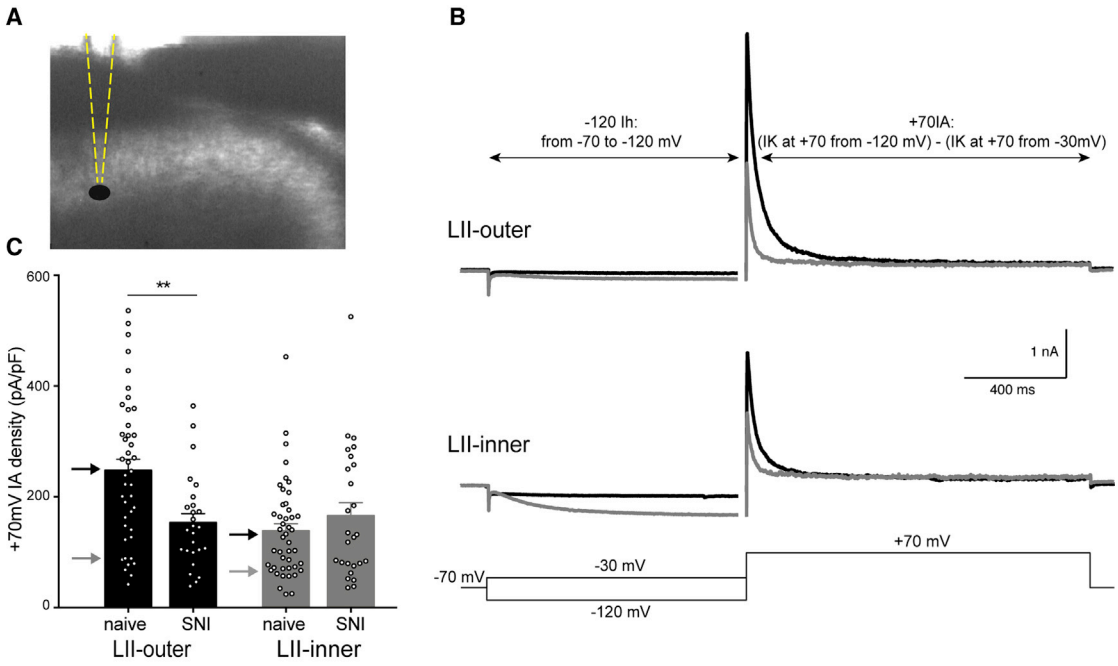

D

Location	Mice model & Neurons numbers	IA (+70 mV; pA)	IA density (+70 mV; pA/pF)	Ih (-120 mV; pA)	Ih density (-120 mV; pA/pF)
LII outer	Naïve (42)	5449 ±380	247 ±20	- 50.2 ±7.0	-2.1 ± 0.3
	SNI (28)	4071 ±477	153 ±16	-87.1 ± 23.8	-3.5 ± 1.0
LII inner	Naïve (45)	3433 ±291	138 ±13	-88.9 ± 12.8	-3.6 ± 0.6
	SNI (26)	3643 ±523	166 ±23	-113 ± 27	-5.3 ± 1.3

Figure 4. Blind whole-cell recordings from L-II INs in WT mice spinal cord slices reveal a decrease in I_A in L-IIo after SNI

(A) Mouse spinal cord slice showing the laminar localization of the recording pipette.

(B) Representative I_h and I_A traces from L-IIo and L-IIi INs in spinal cord slices from WT naive mice. I_h evoked by stepping from −70 to −120 mV is shown on the left, and I_A obtained by offline subtraction ([total K^+ current evoked by stepping from −120 to +70 mV] − [K^+ current evoked by stepping from −30 to +70 mV]) is shown on the right. The black traces were obtained from neurons in which I_A amplitude was close to the total sample mean values (black arrows in B) and that had no I_h. The gray traces were obtained from neurons characterized by an I_A of small amplitude (gray arrows in B) and a large I_h in LIIi.

(C) Comparison of I_A densities (from −120 to +70 mV) in L-IIo and L-IIi INs in WT mice under naive conditions and after SNI. Data are the mean ± SEM for 26–45 neurons. **$p < 0.01$ (unpaired t tests).

(D) Table presenting the mean of I_A and I_A densities (at +70 mV) as well as I_h and I_h densities (at −120 mV) in L-IIo and L-IIi in naive mice or mice submitted to SNI. See also Table S1.

4B and 5B) used to evoke I_A also triggers I_h and T-type Ca^{2+} currents (I_T), but I_T was undetectable here because of its small amplitude. We focused on the Kv4 channels that generate tetraethylammonium chloride (TEA)-resistant I_A by using an extracellular solution containing a high TEA-Cl concentration, as described previously (Strube et al., 2015). We found that, in WT mice, SNI strongly decreased I_A amplitude in L-IIo with no detectable change in the I_A amplitude in L-IIi (Figures 4C and 4D). I_h was extremely small in most L-II neurons (except for a small subpopulation of L-IIi neurons with a small I_A; Figure 4B) and did not appear to be affected by SNI in either of the lamina (Figure 4D).

We then tried to identify the IN subtypes in which the SNI-mediated alteration of I_A occurred, using gad1^{GFP} mice (Tamamaki et al., 2003). In these mice, 95% of inhibitory INs are labeled with GFP, making it possible to discriminate between inhibitory INs (InhINs; GFP^+) and excitatory INs (ExINs; GFP^-) (Figure 5A). We also chose to study these mice for the following two reasons: (1) changes to intrinsic properties might be expected in InhINs because SNI induces alterations to firing patterns and rheobase in the parvalbumin (PV^+) InhINs located in L-III and ventral L-IIi and characterized by a large I_h (Boyle et al., 2019; Hughes et al., 2012), and (2) we hypothesized that the intrinsic electrophysiological properties of L-II-InhINs might be targeted by TAFA4, which is known to enhance GABAergic tone in L-II by increasing the frequency of spontaneous and miniature inhibitory postsynaptic currents (IPSCs) and decreasing the frequency of spontaneous and miniature excitatory postsynaptic currents (EPSCs) with no change in amplitude (Kambrun et al., 2018).

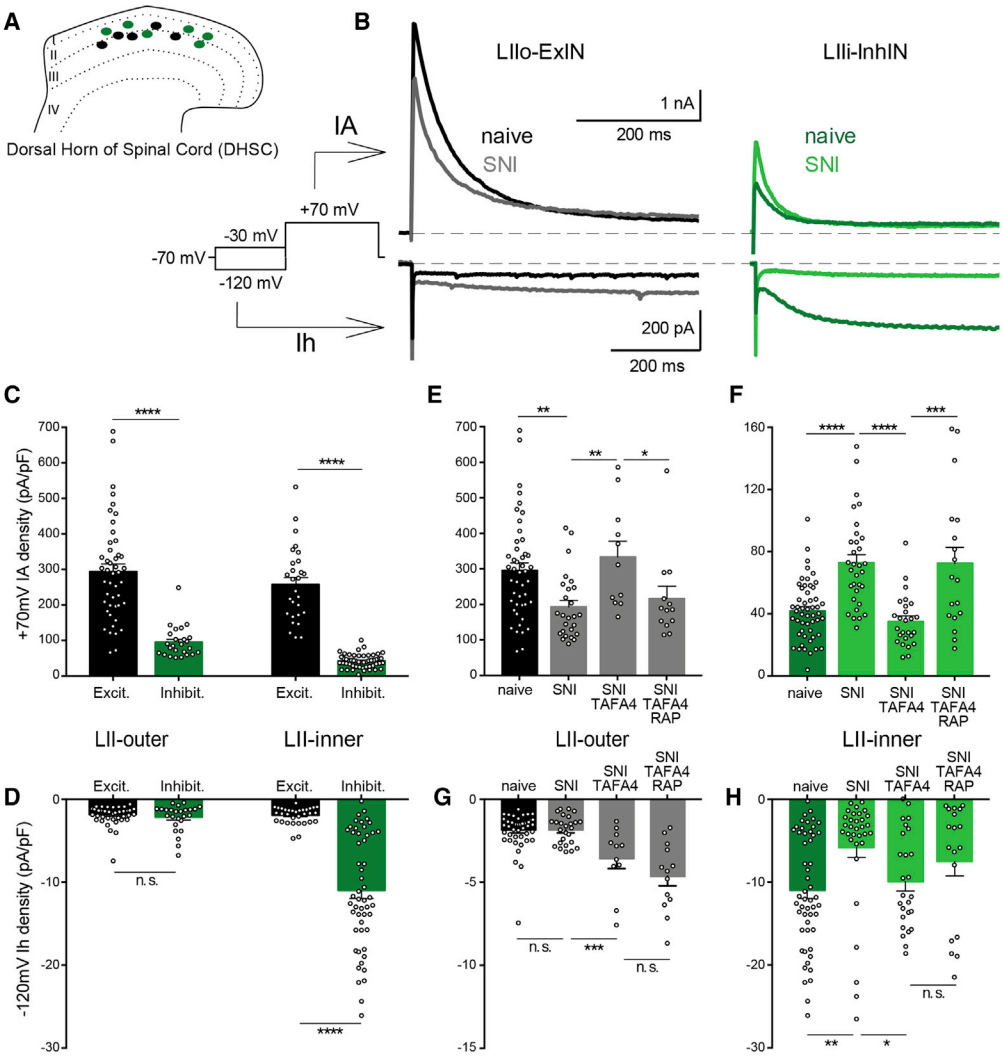

I

Location	neuron type	Mice model & pharmacology (n)	IA (+70 mV; pA)	IA density (+70 mV; pA/pF)	Ih (-120 mV; pA)	Ih density (-120 mV; pA/pF)
LII outer	ExIN	Naïve (46)	6367 ±378	294 ±21	-41.2± 3.3	-1.9±0.2
		SNI (26)	4366 ±430	192 ±18	-41.5±4.4	-1.9±0.2
		SNI; TAFA4 (11)	6078 ±966	333 ±44	-59.9±8.0	-3.6±0.6
		SNI;TAFA4+RAP (13)	3976 ±751	216 ±34	-78.5 ±7.1	-4.7 ±0.6
	InhIN	Naïve (25)	2589 ±227	95.4±8.7	-62.6±10.1	-2.2 ±0.3
		SNI (14)	2589 ±254	84.3±11.2	-52.8±9.5	-1.6±0.3
LII inner	ExIN	Naïve (28)	5997 ±452	258 ±19.9	-44.8 ±3.9	-1.9 ±0.2
		SNI (21)	5348 ±701	245 ±27.5	-45.6 ±7.1	-2.3 ±0.4
	InhIN	Naïve (52)	1405 ±114	42.1 ±2.6	-330.6 ±25.6	-11.0 ±0.9
		Naïve; Cs+Cd (26)	1670 ±155	44.9 ±4.5	-67.3 ±9.2	-1.8 ±0.3
		SNI (32)	2365 ±171	73.1 ±5.1	-168.5 ±29.0	-5.8 ±1.2
		SNI; TAFA4 (26)	1235 ±148	35.3 ±3.2	-309.9 ±32.2	-9.9 ±1.1
		SNI;TAFA4+RAP (18)	1657 ±202	72.5 ±10.4	-191.8 ±48.9	-7.5 ±1.7

(legend on next page)

With this mouse model, we found that I_A amplitudes were much larger in ExINs than in InhINs for L-IIo and L-IIi (Figures 5B, 5C, and 5I). Consistent with our blind recording data, a large I_h (probably carried by HCN1 because it displays rapid activation with a time constant at −120 mV = 205.52 ± 25.79 ms, n = 52) was observed specifically in L-IIi InhINs (Figures 5B, 5D, and 5I). I_h was much smaller in L-IIo InhINs (Figures 5B, 5D, and 5I). Similar low I_h amplitudes were found in L-IIo and L-IIi ExINs (Figures 5D and 5I).

By subjecting gad1^{GFP} mice to SNI, we were able to identify two IN populations displaying alterations to low-threshold ion currents. First, SNI induced a significant decrease in I_A amplitudes in L-IIo ExINs (Figures 5B, 5E, and 5I). Second, more surprisingly, SNI significantly increased I_A amplitudes in L-IIi InhINs (Figures 5B, 5F, and 5I). This increase in I_A amplitudes following SNI in L-IIi InhINs was accompanied by a decrease in I_h amplitude (Figures 5B, 5H, and 5I). We checked that the SNI-induced increase in I_A amplitudes in L-IIi InhIN persisted when the recordings were performed with CsCl (to block I_h) together with 20 μM CdCl (to block Ca^{2+} currents) (Figure 5I). SNI had no effect on I_A amplitudes in L-IIi ExINs or L-IIo InhINs (Figures 5G and 5I). In addition, SNI did not modify I_h in all IN types in which this current was small (Figure 5I).

We then investigated whether TAFA4 could reverse the SNI-mediated alterations in I_A and I_h. Recombinant TAFA4 totally reversed the SNI-induced decrease in I_A in L-IIo ExINs (Figures 5E and 5I). TAFA4 triggered a small but significant increase in I_h in these same INs (Figures 5G and 5I). Recombinant TAFA4 also reversed the SNI-mediated increase in I_A in L-IIi InhINs (Figures 5F and 5I) as well as the SNI-induced decrease in I_h in L-IIi InhIN (Figures 5H and 5I). Finally, consistent with our behavioral pharmacology results, the TAFA4-mediated reversal of the SNI-induced I_A decrease in L-IIo ExINs and increase in L-IIi InhINs was prevented by incubating the spinal cord slices with a mixture of recombinant TAFA4 and RAP (Figures 5E, 5F, 5H, and 5I). RAP addition had no significant effect on TAFA4-mediated modulation of I_h in either of the subsets of INs (Figures 5G–5I).

SNI downregulates TAFA4 in injured DRG neurons and their central terminals

Our findings demonstrate that TAFA4, RAP-sensitive LRPs, HCN1, and A-type Kv channels are key players in modulation of SNI-induced mechanical hypersensitivity. We systematically investigated the effects of SNI on these components by performing a series of qualitative and quantitative analyses on DRGs and DHSC from naive mice and SNI mice 7 days after surgery. We found that SNI had no effect on the levels of transcripts encoding *lrp1*, HCN channels (*hcn1–hcn4*) and all A-type Kv channels (*Kcna4*, *Kcnc 3* and *4*, and *Kcnd1-3*) (Figure S3A). We then performed TAFA4 immunostaining with a newly generated rat anti-mouse-TAFA4 antibody (Hoeffel et al., 2021) on DRG and spinal cord sections from WT and TAFA4-null mice. Standard protocols were used for TAFA4 immunostaining on DRG sections. In contrast, TAFA4 immunostaining on SC sections required special conditions, as described in the STAR methods section. TAFA4 is expressed in a subset of DRG neurons, and, as expected for C-LTMRs, TAFA4$^+$ central terminals project into LIIi, just beneath IB4$^+$ fibers (Figures S3B and S3C). TAFA4 labeling was abolished in both types of samples from TAFA4-null mice, demonstrating the specificity of the anti-TAFA4 antibody.

We used this tool in combination with qRT-PCR, to determine whether SNI affected TAFA4 expression at the transcriptional, translational, or trafficking levels. We first identified the lumbar DRGs affected by the nerve lesion by injecting the cholera toxin B subunit (CTb) into the footpad of the hind paw. Under these conditions, CTb retrogradely labeled myelinated sensory neuron cell bodies located in lumbar 4 and 5 (L4 and L5) DRGs but not in L3, L2, or L1 DRGs (Figure 6A; data not shown). We then performed qRT-PCR on contralateral and ipsilateral L3, L4, and L5 DRGs 7 days after SNI. Consistent with our CTb retro-labeling results, qRT-PCR revealed a significant increase in the abundance of *atf3* transcripts in the ipsilateral L4 and L5 DRGs but not in the L3 DRGs (Figure 6B). Consistent with this finding, SNI induced a significant decrease of *tafa4* transcripts in the ipsilateral L4 and L5 DRGs (Figure 6C), whereas the total number of TAFA4$^+$ neurons in these DRGs was unaffected (Figure 6D). We investigated whether the decrease in *tafa4* transcript levels was accompanied by a decrease in TAFA4 protein levels within C-LTMR L-IIi spinal projections by performing double immunostaining on SC sections from lumbar segments with anti-TAFA4 and anti-Iba1 antibodies. In contrast to what was observed on the contralateral side, SNI completely eliminated the TAFA4 protein from the spinal region where high levels of microglial activation were demonstrated by Iba1 immunoreactivity (Figure 6E).

DISCUSSION

We show here that TAFA4 is endowed with strong potential to reverse pathologically increased mechanical hypersensitivity

Figure 5. SNI-induced alterations of I_A and I_h in L-II IN subsets are reversed by TAFA4 in an LRP-dependent manner

(A) Schematic of mouse spinal cord slices showing laminar localization of the recorded INs.

(B) Representative I_h and I_A traces from L-IIo ExINs and L-IIi InhINs in spinal cord slices from *gad1*^{GFP} mice either naive or submitted to SNI. The upper traces show I_A obtained by offline subtraction ([total K^+ current evoked by stepping from −120 to +70 mV] − [K^+ current evoked by stepping from −30 to +70 mV]), and the bottom traces show I_h evoked by stepping from −70 to −120 mV.

(C and D) Comparison of I_A densities (from −120 to +70 mV; C) and I_h densities (from −70 to −120 mV; D) in ExINs (black) and InhINs (green) patched in L-IIo and L-IIi using *gad1*^{GFP} mice under naive conditions. Results are expressed as mean ± SEM. ****p < 0.0001 (unpaired t tests).

(E–H) Comparison of I_A densities (from −120 to +70 mV; E and F) and I_h densities (from −70 to −120 mV; G and H) in L-IIo ExINs and L-IIi InhINs from naive *gad1*^{GFP} mice or mice submitted to SNI in the presence or absence of TAFA4 with and without RAP antagonism. Results are expressed as mean ± SEM. ****p < 0.0001, ***p < 0.001, **p < 0.01, *p < 0.05 (unpaired t tests).

(I) Table presenting the mean of I_A and I_A densities (from −120 to +70 mV) as well as I_h and I_h densities (from −70 mV to −120 mV) obtained in ExINs and InhINs located in L-IIo and L-IIi of naive *gad1*^{GFP} mice or mice submitted to SNI.

See also Table S1.

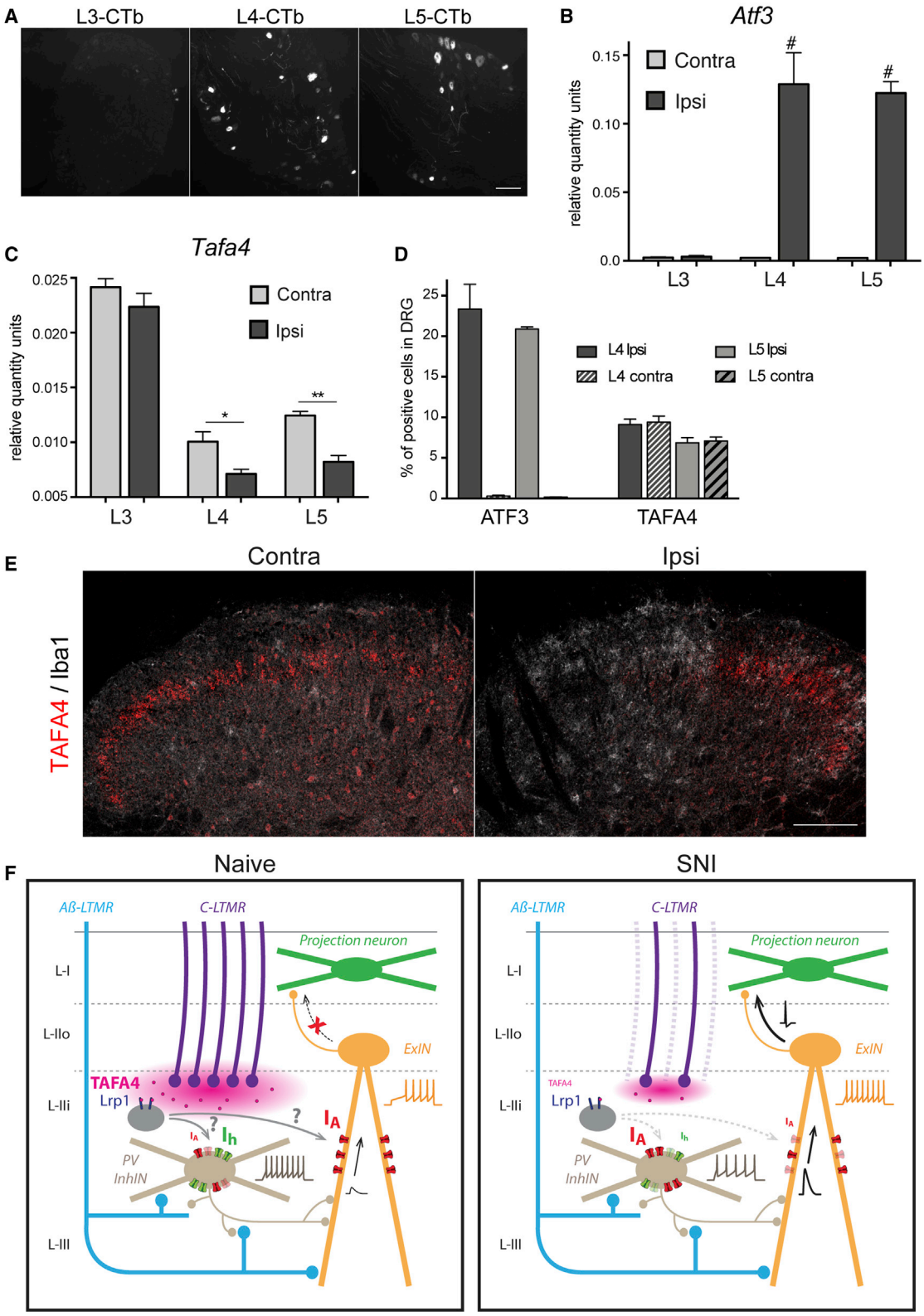

(legend on next page)

and provide insights into its mechanism of action. We show that spinal (IT) or systemic (s.c.) administration of TAFA4 reverses inflammatory, postoperative, and nerve injury-induced mechanical hypersensitivity in male and female mice. We also show that the antihypersensitive actions of TAFA4 require functional RAP-sensitive LRPs. In parallel, we found that exogenous administration of recombinant TAFA4 reverses SNI-induced alterations of the electrophysiological properties of spinal cord INs, including a decrease in I_A in L-IIo ExINs and an increase in I_A together with a decrease in I_h in L-IIi InhINs, strongly suggesting that these changes underlie SNI-induced sensitization.

The decrease in I_A in L-IIo ExINs after SNI reported here has also been observed during inflammation following injection of capsaicin into the hind paw of mice (Zhang et al., 2018). In L-IIo ExINs, in particular L-IIo SOM^{Cre}-negative neurons, I_A is crucial for the timing mechanisms required for gating innocuous Aβ inputs that may activate pain pathways (Zhang et al., 2018). In the inflammation and SNI models, the decrease in I_A in this IN subtype opens the gate to innocuous inputs toward pain pathways. Targeting of this common mechanism by TAFA4 probably accounts for the effects of TAFA4 on inflammatory and SNI-induced mechanical hypersensitivity.

The SNI-induced alterations of subthreshold ion currents in L-IIi InhINs have not been described so far. Remarkably, SNI altered I_h and I_A, in opposite directions (decreasing I_h amplitudes and increasing I_A amplitudes). These two currents have opposite influence on membrane excitability, with the depolarizing action of I_h promoting firing and I_A acting as a brake against firing (Marder and Goaillard, 2006). The SNI-related synergistic modulation of I_h and I_A demonstrated here should, therefore, lead to a strong decrease in the excitability of L-IIi InhINs. The changes in ion currents observed in L-IIo ExINs and in L-IIi InhINs in response to SNI (and reversed by TAFA4) should lead to a strong increase in the responsiveness of the network to incoming inputs because of the synergistic decrease in the excitability of InhINs and increase in that of ExINs.

The incubation of spinal cord slices with recombinant TAFA4 reversed each of the detected ion channel alterations caused by SNI. This reversal occurred after long incubations of the slices with TAFA4 (at least 40 minutes), suggesting the activation of as yet unidentified signaling pathways or cell behaviors restoring the normal function of L-IIo-ExIN and L-IIi-InhIN.

How can exogenous administration of TAFA4 lead to opposite modifications of I_A in L-IIo ExINs and L-IIi InhINs? Two scenarios are possible. (1) TAFA4 may activate different cellular and/or molecular pathways independently targeting I_A in L-IIo ExINs and in L-IIi InhINs, or (2) a single cellular and molecular pathway may be involved, with recombinant TAFA4 preferentially targeting L-IIi InhINs, whose activity modulates I_A levels in L-IIo ExINs. The second scenario was recently put forward by Zhang et al. (2018), who showed that ablation of preprodynorphin-derived neurons induces a significant decrease in I_A in L-IIo ExINs, leading to an increase in the number of L-IIo INs generating fast Aβ-evoked action potentials. Preprodynorphin-derived neurons are necessarily included in our large $gad1^{GFP}$-positive neuron sample, in which only PV^+ neurons could be identified on the basis of their expression of large I_h. It is also possible that PV^+ neuron activity controls I_A size in L-IIo ExINs because these PV neurons target different excitatory neuron subpopulations in L-IIo (Boyle et al., 2019; Petitjean et al., 2015).

Finally, we show here that, in addition to altering spinal IN I_A and I_h, SNI also decreases the levels of TAFA4 in L4 and L5 DRGs and in their corresponding C-LTMRs central terminals.

All of the effects of TAFA4 reported here (reversal of mechanical hypersensitivity and rescue of ion current alterations caused by SNI) require functional RAP-sensitive LRPs. Among these receptors, LRP1 has been shown to play a critical role in the somatosensory system (Gonias and Campana, 2014). Indeed, LRP1 is expressed in neurons (DRGs and SCs), astrocytes, activated microglia, and Schwann cells. LRP1 is a large (600 kDa) cell surface receptor with a broad spectrum of functions. In the context of pain, it may regulate the cellular microenvironment of the injured or inflamed nervous system through endocytosis of various extracellular mediators or by facilitating endocytosis of other transmembrane receptors involved in cell signaling (Gonias and Campana, 2014). Deletion of the LRP1 gene in Schwann cells leads to prolonged partial sciatic nerve ligation (PNL)-induced mechanical hypersensitivity (Orita et al., 2013), whereas deletion of this gene in microglia prevents development of PNL-induced mechanical allodynia by impairing microglial activation (Brifault et al., 2019). Consistent with these findings, we also found that deletion of microglial LRP1 prevents SNI-induced microglial activation and strongly decreases paw incision-induced mechanical hypersensitivity (data not shown).

There is a strong consensus that microglial mediators contribute to regulation of acute and persistent pain by modulating excitatory and inhibitory synaptic transmission in the spinal cord (Ji et al., 2013). For example, tumor necrosis factor alpha (TNF-α) increases the frequency of spontaneous EPSCs (sEPSCs), interleukin-6 (IL-6) decreases the frequency of

Figure 6. SNI induces a significant decreased in C-LTMR-derived TAFA4

(A) Alexa Fluor 647-conjugated CTb, injected into the footpad of the hind paw of mice submitted to SNI, retro-labeled the cell bodies of myelinated primary afferent neurons located in L4 and L5 DRGs but not in L3 DRGs. Scale bar, 100 μm.

(B and C) qRT-PCR highlighting expression of *atf3* and *tafa4* in ipsilateral and Contra L3, L4, and L5 DRGs on day 7 after SNI. SNI induces massive upregulation of *Atf3* and a significant decrease of *tafa4* expression in L4 and L5 but not in L3 DRGs. Results are expressed as mean ± SEM for three independent experiments. $^{**}p < 0.01$, $^{*}p < 0.05$ (unpaired t tests).

(D) Percentage of $ATF3^+$ or $TAFA4^+$ neurons in L4 and L5 ipsilateral and Contra DRGs on day 7 after SNI. Histograms show the mean ± SEM for three mice.

(E) Immunostaining of spinal cord sections showing the distribution of the TAFA4 (red) and Iba1 (white) proteins in Contra (left panels) and ipsilateral (right panels) sections on day 7 after SNI. The ipsilateral immunoreactivity of TAFA4 was abolished in spinal territories with high levels of microglial activation, as shown by Iba1 staining. Scale bar, 100 μm.

(F) Working model summarizing the interplay between C-LTMRs expressing TAFA4, spinal LRP1, and I_A and I_h currents in modulation of Aβ-evoked stimuli under naive conditions and following SNI.

See also Figure S3.

spontaneous inhibitory postsynaptic currents (sIPSCs), and IL-1β acts on sEPSCs and sIPSCs by increasing (for sEPSCs) and decreasing (for sIPSCs) their frequency and amplitude (Kawasaki et al., 2008). Consistent with these findings, we have shown that bath applications of recombinant TAFA4 enhance inhibitory synaptic transmission within the spinal network by promoting microglial retraction and increasing the number of inhibitory synapses on L-IIi somata (Kambrun et al., 2018). We show here that inhibition of spinal RAP-sensitive LRPs completely abolishes the TAFA4-mediated reversal of mechanical hypersensitivity in the SNI and paw incision pain models. Given the crucial role of microglial LRP1 in modulation of nerve injury (Brifault et al., 2019) and in the paw incision model (unpublished data), we favor the hypothesis that TAFA4 mediates its antihypersensitive actions by decreasing secretion of microglial mediators and restoring normal excitatory and inhibitory neurotransmission. In line with this, we recently showed that TAFA4 increases production of the anti-inflammatory cytokine IL-10 by dermal macrophages after UV radiation-induced skin damage, reducing skin inflammation and promoting tissue regeneration (Hoeffel et al., 2021). We thus propose a model where, under pathological conditions such as SNI (Figure 6F, right panel), exogenously administered TAFA4 restores the gating activity of L-IIi InhINs by reversing the SNI-mediated increase of I_A and decrease of I_h, mimicking physiological conditions where low-threshold mechanical stimuli are prevented to access the pain pathway (Figure 6F, left panel). Therefore, TAFA4 is not only a strong candidate treatment for injury-induced mechanical hypersensitivity but also a powerful physiological regulator whose tone may restore an appropriate balance between excitation and inhibition in the spinal cord network under physiological conditions.

STAR★METHODS

Detailed methods are provided in the online version of this paper and include the following:

- KEY RESOURCES TABLE
- RESOURCE AVAILABILITY
  - Lead contact
  - Materials availability
  - Data and code availability
- EXPERIMENTAL MODEL AND SUBJECT DETAILS
  - Mice
- METHOD DETAILS
  - Pain models
  - Behavioral tests
  - Drugs and *in vivo* administration methods
  - Cell lines and DNA constructs
  - Recombinant protein production and extraction
  - Pulldown assay
  - Intracellular calcium mobilization assay
  - β-arrestin BRET assay
  - Antibodies and reagents
  - Tissue processing for immunofluorescence (IF)
  - Immunofluorescence
  - Cell surface binding assay
  - Enzyme-linked binding assay
  - Slice preparation and treatment for electrophysiological recordings
  - Patch-clamp recordings
  - Data acquisition and analysis
  - Reverse transcription- quantitative polymerase chain reaction: RT-qPCR
- QUANTIFICATION AND STATISTICAL ANALYSIS

SUPPLEMENTAL INFORMATION

Supplemental information can be found online at https://doi.org/10.1016/j.celrep.2021.109884.

ACKNOWLEDGMENTS

We thank the members of the Moqrich laboratory for fruitful scientific discussions. This work was funded by the French National Research Agency (ANR-CE16-Myochronic to A.M.), a "Fondation pour la Recherche Médicale (FRM)" postdoctoral fellowship (to S.Y.), Equipe FRM-EQP202003010192 (to A.M.), and Biotrail PhD funding (to C.S.). This work was also supported by institutional funding from CNRS and Aix-Marseille-Université (to IBDM).

AUTHOR CONTRIBUTIONS

S.Y. generated all electrophysiology data and contributed to their analysis. C.S. performed all behavioral experiments. A.R. designed and performed qRT-PCR on DRGs and spinal cord and immunostaining for the quantification experiments. I.M. performed hFC-TAFA4 binding experiments. P.M. managed the mouse colonies used in this study and performed all qRT-PCR experiments. S.G. performed several behavioral experiments not presented here. A.C. contributed to unpublished data. S.U. and R.R. generated and validated the anti-TAFA4 antibody. A.E.K. contributed to validation of the TAFA4/LRP1 interaction. J.-Y.S. and M.P. designed and performed the BRET and calcium mobilization experiments. A.J.S. contributed to unpublished data. J.-M.G. participated in writing of the discussion of the electrophysiological data, designed the working model, and provided major input for the manuscript. F.C. designed and performed all biochemistry experiments and produced all figures. N.C. designed the electrophysiological experiments, analyzed all electrophysiological data, and participated in writing of the manuscript. A.M. conceived the project and wrote the manuscript.

DECLARATION OF INTERESTS

A.M. and S.G. are exploiting TAFA4 patent number DI 06104-01 to launch a start-up company, Tafalgie Therapeutics, with the aim of performing clinical trials on the use of TAFA4 to treat postoperative pain.

INCLUSION AND DIVERSITY

We worked to ensure sex balance in the selection of non-human subjects.

Received: March 2, 2021
Revised: July 30, 2021
Accepted: October 5, 2021
Published: October 26, 2021

REFERENCES

Ackerley, R., Carlsson, I., Wester, H., Olausson, H., and Backlund Wasling, H. (2014). Touch perceptions across skin sites: differences between sensitivity, direction discrimination and pleasantness. Front. Behav. Neurosci. *8*, 54.

Benyamin, R., Trescot, A.M., Datta, S., Buenaventura, R., Adlaka, R., Sehgal, N., Glaser, S.E., and Vallejo, R. (2008). Opioid complications and side effects. Pain Physician *11* (*2, Suppl*), S105–S120.

Boscia, F., Esposito, C.L., Casamassa, A., de Franciscis, V., Annunziato, L., and Cerchia, L. (2013). The isolectin IB4 binds RET receptor tyrosine kinase in microglia. J. Neurochem. *126*, 428–436.

Bourane, S., Duan, B., Koch, S.C., Dalet, A., Britz, O., Garcia-Campmany, L., Kim, E., Cheng, L., Ghosh, A., Ma, Q., and Goulding, M. (2015a). Gate control of mechanical itch by a subpopulation of spinal cord interneurons. Science *350*, 550–554.

Bourane, S., Grossmann, K.S., Britz, O., Dalet, A., Del Barrio, M.G., Stam, F.J., Garcia-Campmany, L., Koch, S., and Goulding, M. (2015b). Identification of a spinal circuit for light touch and fine motor control. Cell *160*, 503–515.

Boyle, K.A., Gradwell, M.A., Yasaka, T., Dickie, A.C., Polgár, E., Ganley, R.P., Orr, D.P.H., Watanabe, M., Abraira, V.E., Kuehn, E.D., et al. (2019). Defining a Spinal Microcircuit that Gates Myelinated Afferent Input: Implications for Tactile Allodynia. Cell Rep. *28*, 526–540.e6.

Brennan, T.J. (1999). Postoperative Models of Nociception. ILAR J. *40*, 129–136.

Brifault, C., Kwon, H., Campana, W.M., and Gonias, S.L. (2019). LRP1 deficiency in microglia blocks neuro-inflammation in the spinal dorsal horn and neuropathic pain processing. Glia *67*, 1210–1224.

Colloca, L., Ludman, T., Bouhassira, D., Baron, R., Dickenson, A.H., Yarnitsky, D., Freeman, R., Truini, A., Attal, N., Finnerup, N.B., et al. (2017). Neuropathic pain. Nat. Rev. Dis. Primers *3*, 17002.

Corbisier, J., Galès, C., Huszagh, A., Parmentier, M., and Springael, J.Y. (2015). Biased signaling at chemokine receptors. J. Biol. Chem. *290*, 9542–9554.

Costigan, M., Scholz, J., and Woolf, C.J. (2009). Neuropathic pain: a maladaptive response of the nervous system to damage. Annu. Rev. Neurosci. *32*, 1–32.

Coull, J.A., Beggs, S., Boudreau, D., Boivin, D., Tsuda, M., Inoue, K., Gravel, C., Salter, M.W., and De Koninck, Y. (2005). BDNF from microglia causes the shift in neuronal anion gradient underlying neuropathic pain. Nature *438*, 1017–1021.

Decosterd, I., and Woolf, C.J. (2000). Spared nerve injury: an animal model of persistent peripheral neuropathic pain. Pain *87*, 149–158.

Delfini, M.C., Mantilleri, A., Gaillard, S., Hao, J., Reynders, A., Malapert, P., Alonso, S., François, A., Barrere, C., Seal, R., et al. (2013). TAFA4, a chemokine-like protein, modulates injury-induced mechanical and chemical pain hypersensitivity in mice. Cell Rep. *5*, 378–388.

Duan, B., Cheng, L., Bourane, S., Britz, O., Padilla, C., Garcia-Campmany, L., Krashes, M., Knowlton, W., Velasquez, T., Ren, X., et al. (2014). Identification of spinal circuits transmitting and gating mechanical pain. Cell *159*, 1417–1432.

El-Asmar, L., Springael, J.Y., Ballet, S., Andrieu, E.U., Vassart, G., and Parmentier, M. (2005). Evidence for negative binding cooperativity within CCR5-CCR2b heterodimers. Mol. Pharmacol. *67*, 460–469.

Gonias, S.L., and Campana, W.M. (2014). LDL receptor-related protein-1: a regulator of inflammation in atherosclerosis, cancer, and injury to the nervous system. Am. J. Pathol. *184*, 18–27.

Herz, J., Clouthier, D.E., and Hammer, R.E. (1992). LDL receptor-related protein internalizes and degrades uPA-PAI-1 complexes and is essential for embryo implantation. Cell *71*, 411–421.

Hoeffel, G., Debroas, G., Roger, A., Rossignol, R., Gouilly, J., Laprie, C., Chasson, L., Barbon, P.V., Balsamo, A., Reynders, A., et al. (2021). Sensory neuron-derived TAFA4 promotes macrophage tissue repair functions. Nature *594*, 94–99.

Hu, H.J., Carrasquillo, Y., Karim, F., Jung, W.E., Nerbonne, J.M., Schwarz, T.L., and Gereau, R.W., 4th. (2006). The kv4.2 potassium channel subunit is required for pain plasticity. Neuron *50*, 89–100.

Hughes, D.I., Sikander, S., Kinnon, C.M., Boyle, K.A., Watanabe, M., Callister, R.J., and Graham, B.A. (2012). Morphological, neurochemical and electrophysiological features of parvalbumin-expressing cells: a likely source of axo-axonic inputs in the mouse spinal dorsal horn. J. Physiol. *590*, 3927–3951.

Ji, R.R., Berta, T., and Nedergaard, M. (2013). Glia and pain: is chronic pain a gliopathy? Pain *154* (*Suppl 1*), S10–S28.

Kambrun, C., Roca-Lapirot, O., Salio, C., Landry, M., Moqrich, A., and Le Feuvre, Y. (2018). TAFA4 Reverses Mechanical Allodynia through Activation of GABAergic Transmission and Microglial Process Retraction. Cell Rep. *22*, 2886–2897.

Kawasaki, Y., Zhang, L., Cheng, J.K., and Ji, R.R. (2008). Cytokine mechanisms of central sensitization: distinct and overlapping role of interleukin-1beta, interleukin-6, and tumor necrosis factor-alpha in regulating synaptic and neuronal activity in the superficial spinal cord. J. Neurosci. *28*, 5189–5194.

Keyhanfar, F., Shamsi Meymandi, M., Sepehri, G., Rastegaryanzadeh, R., and Heravi, G. (2013). Evaluation of Antinociceptive Effect of Pregabalin in Mice and its Combination with Tramadol using Tail Flick Test. Iran. J. Pharm. Res. *12*, 483–493.

Khalaj, A.J., Sterky, F.H., Sclip, A., Schwenk, J., Brunger, A.T., Fakler, B., and Südhof, T.C. (2020). Deorphanizing FAM19A proteins as pan-neurexin ligands with an unusual biosynthetic binding mechanism. J. Cell Biol. *219*, e202004164.

Lee, D., Walsh, J.D., Migliorini, M., Yu, P., Cai, T., Schwieters, C.D., Krueger, S., Strickland, D.K., and Wang, Y.X. (2007). The structure of receptor-associated protein (RAP). Protein Sci. *16*, 1628–1640.

Li, L., Rutlin, M., Abraira, V.E., Cassidy, C., Kus, L., Gong, S., Jankowski, M.P., Luo, W., Heintz, N., Koerber, H.R., et al. (2011). The functional organization of cutaneous low-threshold mechanosensory neurons. Cell *147*, 1615–1627.

Liu, Q., Trotter, J., Zhang, J., Peters, M.M., Cheng, H., Bao, J., Han, X., Weeber, E.J., and Bu, G. (2010). Neuronal LRP1 knockout in adult mice leads to impaired brain lipid metabolism and progressive, age-dependent synapse loss and neurodegeneration. J. Neurosci. *30*, 17068–17078.

Löken, L.S., Wessberg, J., Morrison, I., McGlone, F., and Olausson, H. (2009). Coding of pleasant touch by unmyelinated afferents in humans. Nat. Neurosci. *12*, 547–548.

Marder, E., and Goaillard, J.M. (2006). Variability, compensation and homeostasis in neuron and network function. Nat. Rev. Neurosci. *7*, 563–574.

Marschang, P., Brich, J., Weeber, E.J., Sweatt, J.D., Shelton, J.M., Richardson, J.A., Hammer, R.E., and Herz, J. (2004). Normal development and fertility of knockout mice lacking the tumor suppressor gene LRP1b suggest functional compensation by LRP1. Mol. Cell. Biol. *24*, 3782–3793.

McGlone, F., Wessberg, J., and Olausson, H. (2014). Discriminative and affective touch: sensing and feeling. Neuron *82*, 737–755.

Olausson, H., Lamarre, Y., Backlund, H., Morin, C., Wallin, B.G., Starck, G., Ekholm, S., Strigo, I., Worsley, K., Vallbo, A.B., and Bushnell, M.C. (2002). Unmyelinated tactile afferents signal touch and project to insular cortex. Nat. Neurosci. *5*, 900–904.

Orita, S., Henry, K., Mantuano, E., Yamauchi, K., De Corato, A., Ishikawa, T., Feltri, M.L., Wrabetz, L., Gaultier, A., Pollack, M., et al. (2013). Schwann cell LRP1 regulates remak bundle ultrastructure and axonal interactions to prevent neuropathic pain. J. Neurosci. *33*, 5590–5602.

Peirs, C., Williams, S.P., Zhao, X., Walsh, C.E., Gedeon, J.Y., Cagle, N.E., Goldring, A.C., Hioki, H., Liu, Z., Marell, P.S., and Seal, R.P. (2015). Dorsal Horn Circuits for Persistent Mechanical Pain. Neuron *87*, 797–812.

Petitjean, H., Pawlowski, S.A., Fraine, S.L., Sharif, B., Hamad, D., Fatima, T., Berg, J., Brown, C.M., Jan, L.Y., Ribeiro-da-Silva, A., et al. (2015). Dorsal Horn Parvalbumin Neurons Are Gate-Keepers of Touch-Evoked Pain after Nerve Injury. Cell Rep. *13*, 1246–1257.

Petitjean, H., Bourojeni, F.B., Tsao, D., Davidova, A., Sotocinal, S.G., Mogil, J.S., Kania, A., and Sharif-Naeini, R. (2019). Recruitment of Spinoparabrachial Neurons by Dorsal Horn Calretinin Neurons. Cell Rep. *28*, 1429–1438.e4.

Sarver, D.C., Lei, X., and Wong, G.W. (2021). FAM19A (TAFA): An Emerging Family of Neurokines with Diverse Functions in the Central and Peripheral Nervous System. ACS Chem. Neurosci. *12*, 945–958.

Seal, R.P., Wang, X., Guan, Y., Raja, S.N., Woodbury, C.J., Basbaum, A.I., and Edwards, R.H. (2009). Injury-induced mechanical hypersensitivity requires C-low threshold mechanoreceptors. Nature *462*, 651–655.

Strube, C., Saliba, L., Moubarak, E., Penalba, V., Martin-Eauclaire, M.F., Tell, F., and Clerc, N. (2015). Kv4 channels underlie A-currents with highly variable inactivation time courses but homogeneous other gating properties in the nucleus tractus solitarii. Pflugers Arch. *467*, 789–803.

Tamamaki, N., Yanagawa, Y., Tomioka, R., Miyazaki, J., Obata, K., and Kaneko, T. (2003). Green fluorescent protein expression and colocalization with calretinin, parvalbumin, and somatostatin in the GAD67-GFP knock-in mouse. J. Comp. Neurol. *467*, 60–79.

Tom Tang, Y., Emtage, P., Funk, W.D., Hu, T., Arterburn, M., Park, E.E., and Rupp, F. (2004). TAFA: a novel secreted family with conserved cysteine residues and restricted expression in the brain. Genomics *83*, 727–734.

Wang, W., Li, T., Wang, X., Yuan, W., Cheng, Y., Zhang, H., Xu, E., Zhang, Y., Shi, S., Ma, D., and Han, W. (2015). FAM19A4 is a novel cytokine ligand of formyl peptide receptor 1 (FPR1) and is able to promote the migration and phagocytosis of macrophages. Cell. Mol. Immunol. *12*, 615–624.

Zeilhofer, H.U., Wildner, H., and Yévenes, G.E. (2012). Fast synaptic inhibition in spinal sensory processing and pain control. Physiol. Rev. *92*, 193–235.

Zhang, Y., Liu, S., Zhang, Y.Q., Goulding, M., Wang, Y.Q., and Ma, Q. (2018). Timing Mechanisms Underlying Gate Control by Feedforward Inhibition. Neuron *99*, 941–955.e4.

STAR★METHODS

KEY RESOURCES TABLE

REAGENT or RESOURCE	SOURCE	IDENTIFIER
Antibodies		
Goat anti-Iba1 (1:500)	Abcam	#ab5076
Rabbit anti-ATF3 (1:200)	Santa Cruz Biotechnology	#SC-188
Rat anti-LRP1 (1:300)	Abcam	#ab92544
Guinea pig anti-VGLUT3 (1:500)	Synaptic Systems	#135204
Sheep anti-GFP (for WB 1:4000)	MRC PPU reagent, University of Dundee, UK,	#S268
Chicken anti-GFP (for immunostaining 1:1000)	Thermo Fisher Scientific	#A10262
Rat anti-TAFA4 (1:1000)	Hoeffel et al., 2021	Hoeffel et al., 2021
Chemicals, peptides, and recombinant proteins		
TAFA4	Biotechne	5099-TA-050
RAP	Sigma-Aldrich	553506-50UG
fMLF	Sigma-Aldrich	F3806
Baclofen	Sigma-Aldrich	B5399-500MG
SNC-80	Tocris Bioscience	Catalog No.: 0764
DAMGO	Sigma Aldrich	E7384
Experimental models: Cell lines		
RAW 264.7	ATTC	TIB-71
HEK293	ATTC	CRL-1573.3
CHO-K1	ATTC	CCL-61
Experimental models: Organisms/strains		
C57/Bl6 mice	Charles River Laboratories	000664
Gad1$^{GFP/+}$	Tamamaki et al., 2003	N/A
Tafa4$^{venus/venus}$	Delfini et al., 2013	N/A
Recombinant DNA		
TAFA4-pGEX-4T2	Sigma-Aldrich	GE28-9545-50
LRP1-DII- pEGFP-C2	Addgene	Source Clontech
LRP1-DIII- pEGFP-C2	Addgene	Source Clontech
LRP1-DIV- pEGFP-C2	Addgene	Source Clontech
Softaware and algorithms		
ImageJ	Charles River Laboratories	000664
Zen Blue	Carl Zeiss, Germany	https://www.zeiss.com/microscopy/int/products/microscope-software/zen.html
Clampfit 10.3	Molecular Devices	N/A
SigmaPlot 12	Systat Software Inc. San Jose, CA	N/A

RESOURCE AVAILABILITY

Lead contact

Further information and requests for resources and reagents should be directed to and will be fulfilled by the Lead Contact Aziz Moqrich (aziz.moqrich@univ-amu.fr).

Materials availability

This study did not generate new unique reagents.

Data and code availability

All data reported in this paper will be shared by the lead contact upon request.

This paper does not report original code.

Any additional information required to reanalyze the data reported in this paper is available from the lead contact upon request.

EXPERIMENTAL MODEL AND SUBJECT DETAILS

Mice

C57/Bl6J mice (4 to12 weeks of age) were bought from Charles River Laboratories. *Gad1*$^{GFP/+}$ mice (Tamamaki et al., 2003) were generated by crossing *gad1*$^{GFP/+}$ males with C57/Bl6J females, and were used for experiments at four to five weeks of age. Mice of both sexes were used for all experiments. As no differences were noted between males and females, the data for the two sexes were then combined. Mice were maintained under standard housing conditions (22°C, 40% humidity, 12 h light cycles, and free access to food and water). Particular efforts were made to minimize the number of mice used in this study, and the stress and suffering to which they were subjected. All experiments were conducted in line with the European guidelines for the care and use of laboratory animals (Council Directive 86/609/EEC). All experimental procedures were approved by an independent ethics committee for animal experimentation (APAFIS), as required by the French law and in accordance with the relevant institutional regulations of French legislation on animal experimentation, under license number 2015070217242262-V5#1537. All experiments were performed in accordance with the ARRIVE guidelines.

METHOD DETAILS

Pain models

SNI

The spared nerve injury (SNI) model of peripheral nerve injury was implemented as previously described (Decosterd and Woolf, 2000). Briefly, mice were anesthetized with ketamine (40 mg/kg IP) and xylazine (5 mg/kgIP) and the left sciatic nerve was exposed under aseptic conditions. The distal trifurcation of the sciatic nerve was identified and the tibial and common peroneal branches were ligated with polypropylene nonabsorbable 6-0 sutures (Ethicon); 1 mm was cut out, leaving the sural branch intact. The wound was closed with sutures, and the animals were allowed to recover and returned to their cages.

Paw incision

Paw incision surgery was performed as described by Brennan (1999). Mice were anesthetized with ketamine (40 mg/kg IP) and xylazine (5 mg/kg IP) and a longitudinal incision was made through the skin and fascia of the right hind paw. Forceps were used to elevate the flexor digitorum brevis muscle longitudinally and an incision was made through the muscle with a scalpel, to cut it into two halves. The wound was closed with sutures, and the animals were allowed to recover and returned to their cages.

Carrageenan injection

We injected 20 μL of 1% λ -carrageenan (Sigma-Aldrich, 22049-5G-F) in 1 x PBS into the plantar surface of the left hind paw of the mouse with a Hamilton syringe.

Behavioral tests

All behavioral assays were conducted on 8- to 12-week-old C57/Bl6J mice. Animals were acclimated to their testing environment for 45-60 minutes before each experiment, and all experiments were performed at room temperature (~22°C). Experimenters were blind to the treatments used.

Von Frey's test

Mice were placed in plastic chambers on a wire mesh grid and stimulated with von Frey filaments (Bioseb) by the up-down method (45) starting with a 1 g filament, and using 0.07 and 2 g filaments as the cutoffs.

Open Field test

The Open-fiel apparatus consists of an empty square arena (40X40X35 cm), surrounded by to prevent the animal from escaping. Light inside the arena was unifrm and kept at approximately 100-lux throughtout the tests. Mice were individually placed in the center of the arena and their behavior was recorded using the EthoVision XT16 video-tracking system (Noldus, Inc., Leesburg, VA) over a 60 minutes period. The total distance traveled and the total amount of time spent in the peripheral borders and in the center were recorded. This experiment was done on naive and SNI mice that received a subcutaneous injection of vehicle or 0.3 mg/kg of TAFA4.

Tail-flick test

The tail-flick examination was used to calculate analgesic activity according to the method defined by (Keyhanfar et al., 2013). A radiant heat automatic tail-flick analgesiometer (Bioseb) was used to measure reaction times. The basal reaction time of animals in response to radiant heat was determined by placing the tail on the radiant heat source and recording the time until the tail was removed. A cutoff time of 8 s was used, to prevent tail damage.

Drugs and *in vivo* administration methods

TAFA4 (Biotechne) was dissolved in 0.1 M phosphate buffer (PB); baclofen (Sigma-Aldrich) was dissolved in H_2O (pH 7.6), SNC80 (Tocris Bioscience) was dissolved in 100 mM HCl and DAMGO (Sigma Aldrich) was dissolved in 0.9% NaCl. RAP (Sigma-Aldrich) was dissolved in 0.1 M PB and N-formyl-Met-Leu-Phe (fMLF), Sigma) was dissolved in 2.5% DMSO.

Drugs were administered intrathecally (IT) or systemically using subcutaneous (SC) injections in the neck of the mice, as indicated in the figure legends. For IT injections, 10 μL of each compound was injected into non-anesthetized mice. Successful placement of the needle was confirmed by a slight flick of the tail.

Cell lines and DNA constructs

RAW 264.7 macrophages and HEK293 cells lines were obtained from ATTC.

Nucleotide fragments encoding the LRP1 signal peptide (amino acids (aa) 1 to 21), domain II (aa 788 to 1185), domain III (aa 2467 to 2924) and domain IV (aa 3278 to 3779) were obtained by the RT-PCR amplification (Superscript III and Phusion Hi-Fi DNA polymerase, Thermo Fisher Scientific) of RNA extracted from C57/Bl6JRj mouse brain (RNaesy mini kit, QIAGEN) according to the manufacturer's instructions. PCR products were inserted into pEGFP-C2 plasmids with In-Fusion Cloning technology (Addgene) to produce pLRP1-sD-II-GFP, pLRP1-sD-III-GFP and pLRP1-sD-IV-GFP. These plasmids expressed secreted forms of domains II, III and IV of mouse LRP1 tagged with EGFP.

The mouse TAFA4 nucleotide sequence devoid of signal peptide (coding aa 30 to 135) was amplified by PCR (Phusion Hi-Fi DNA polymerase, Thermo Fisher Scientific) and inserted between the BamHI and NotI sites of the pGEX-4T2 vector to produce GST-TAFA4. All constructs were verified by DNA sequencing (Eurofins Genomics).

Recombinant protein production and extraction

GST-tagged proteins were produced in *Escherichia coli* strain BL21 cultured overnight in 2YT medium at 30°C. Bacterial pellets were resuspended in TBS-Triton buffer (50 mM Tris-HCl pH 7.4, 150 mM NaCl, 1 mM EDTA, 1% Triton X-100 and the Roche cOmplete EDTA-free protease inhibitor cocktail) and bacteria were lysed with a French press followed by sonication at 4°C. Soluble proteins were separated from cell debris by centrifugation and stored at −80°C until use.

HEK293 cells were transfected with pLRP1-sDomII-GFP, pLRP1-sDomIII-GFP and pLRP1-sDomIV-GFP in the presence of Lipofectamine 2000, according to the manufacturer's instructions (Life Technologies). Two days after transfection, the supernatants of the cell cultures were collected, centrifuged to eliminate cells debris and stored at −80°C until use.

Pulldown assay

Bacterial lysates expressing GST, GST TAFA4 or GST-RAP (kindly provided by Jérôme Terrand, CNRS UMR 7021, Strasbourg, France) were incubated for 2 h at 4°C with glutathione-Sepharose 4B beads (GE Healthcare). The beads were thoroughly washed and incubated overnight at 4°C with HEK293 cell culture supernatants containing sDomII-GFP, sDomIII-GFP or sDomIV-GFP. They were then thoroughly washed again, and the proteins retained on the beads were analyzed by sodium dodecyl sulfate–polyacrylamide gel electrophoresis (SDS-PAGE) and western blotting (WB).

Intracellular calcium mobilization assay

Calcium mobilization was measured in CHO-K1 cells stably expressing apoaequorin, Gα16, and the receptor of interest, as previously described (El-Asmar et al., 2005). Cells were incubated for four hours in the dark in the presence of 5 μM coelenterazine h (Promega), then diluted to the appropriate cell density before use. The cell suspension (25,000 cells/well) was added to the wells of 96-well microplates (236108, Nunc) containing the ligands and luminescence was recorded for 30 s in an EG&G Berthold luminometer (PerkinElmer Life Sciences).

β-arrestin BRET assay

β-arrestin recruitment was measured in a BRET proximity assay, as previously described (Corbisier et al., 2015). Plasmids encoding *Renilla* luciferase-tagged β-arrestin 2 (RLuc-β-arrestin 2) and EYFP-tagged FPR1 were used for the cotransfection of HEK293T cells by using the calcium phosphate method. Twenty-four hours post-transfection, cells were collected and used to seed (25,000 cells/well) 96-well microplates (165306, Nunc). They were cultured for an additional 24 h. Cells were then rinsed once with PBS and incubated in PBS plus 0.1% (w/v) glucose. BRET between RLuc and EYFP was measured after the addition of 5 μM coelenterazine h (Promega). Ligands were added 5 min after coelenterazine h and BRET readings were recorded after 30 minutes, with a Mithras LB940 Multilabel Reader (Berthold Technologies). The BRET signal was calculated as the ratio of EYFP emission (520–570 nm) to RLuc emission (370–480 nm).

Antibodies and reagents

The primary antibodies used were: goat anti-Iba1 (1:500, Abcam, #ab5076); rabbit anti-ATF3 (1:200, Santa Cruz Biotechnology, #SC-188), rat anti-LRP1 (1:300, Abcam, #ab92544); guinea pig anti-VGLUT3 (1:500, Synaptic Systems, #135204); sheep anti-GFP (for WB, 1:4000, MRC PPU reagent, University of Dundee, UK, #S268), chicken anti-GFP (for immunostaining 1:1000, Thermo Fisher Scientific, #A10262), and rat anti-TAFA4 (1:1000, clone 1D8, (Hoeffel et al., 2021). The secondary antibodies used for detection of the

primary antibodies were: goat anti-human Fc-Alexa488 (1:300, Jackson, 109-545-098), goat anti-human Fc-HRP (1:2000, Thermo Fisher Scientific, A 188-17), donkey anti-rabbit, anti-rat, anti-guinea pig, anti-chicken and anti-goat antibodies conjugated to Alexa Fluor 488, 555, or 647 (Thermo Fisher Scientific or Molecular Probes antibodies). Isolectin binding 4 (IB4) conjugated to Alexa Fluor 488 was used at a dilution of 1:300 (Thermo Fisher Scientific, #I21411 and #I32450). Recombinant proteins were purchased from Interchim: FAM19A4-hFc Tag (Sino Biological, 11165-H01H), hFc (Sino Biological,10702-HNAC).

Tissue processing for immunofluorescence (IF)

Mice were deeply anesthetized with 100 mg/kg ketamine plus 10 mg/kg xylazine. They were intracardially perfused with 0.1 M phosphate buffer (PB) followed by 4% paraformaldehyde (PFA; in PB). The spinal cord lumbar region and DRGs were dissected, and post-fixed by overnight incubation in the same fixative at 4°C. Fixed tissues were transferred to 30% sucrose in PBS solution and incubated at 4°C until they sank. They were then frozen in OCT medium. We cut 14 to 20 μm-thick sections on a cryostat (Leica). These sections were mounted on Superfrost slides and kept at −80°C until their use for IF experiments.

For TAFA4 detection in the spinal cord, mice were deeply anesthetized with 100 mg/kg ketamine plus 10 mg/kg xylazine, intracardially perfused with ice-cold solution 1 (see Table S1; pH 7.4 through which O_2 was bubbled. The spinal cord lumbar region was dissected in ice-cold solution 1 under continuous oxygenation and immediately frozen in OCT medium. We cut 20 μm-thick sections on a cryostat (Leica), and these sections were mounted on Superfrost slides maintained within the cryostat. Sections were immediately fixed by incubation in 4% PFA for 15 minutes and processed for immunostaining.

Immunofluorescence

Slides were washed for 5 minutes (min) in PBS, incubated for 1 h at room temperature with a blocking solution (10% normal donkey serum, 1% BSA, 0.4% Triton X-100, in PBS), and then overnight at 4°C with primary antibodies in the same blocking solution.

For TAFA4 immunostaining, saturation, and incubations with the primary and secondary antibodies were performed in 3% BSA with no serum or detergents.

Images were acquired with a Zeiss AxioImager M2 fluorescence microscope or a Zeiss LSM 780 confocal microscope, with a 20x, 25x or 63x objective and appropriate excitation wavelengths and emission filters. Laser power and acquisition settings were kept constant between image acquisitions for different conditions. Images were analyzed with ImageJ software.

Cell surface binding assay

RAW264.7 cells were cultured in DMEM supplemented with 100 U/ml penicillin, 100 μg/ml streptomycin, 0.2 mg/ml glutamine and 10% v/v heat-inactivated fetal calf serum (FCS) (Life Technologies) at 37°C, under an atmosphere containing 5% CO^2. They were passaged enzymatically at a 1:10 ratio every five to six days. One day before the binding assay, the cells were plated at a density of 10^5 cells/ml on glass coverslips coated with 100 μg/ml poly-L-lysine (PLL, Sigma-Aldrich).

The surface labeling of TAFA4 receptors was assessed by incubating cells for 1 h at 4°C for 1H with 50 nM TAFA-Fc (Interchim, 11165-H01H) or 50 nM Fc (Interchim, 10702-HNAC) recombinant proteins diluted in 10% FCS in PBS. Cells were then washed with PBS and fixed by incubation with 4% paraformaldehyde (PFA) in PBS for 20 minutes. Cells were incubated with the blocking solution (10% normal donkey serum, 1% BSA, 0.4% Triton X-100, in PBS) for 1 hour and then overnight at 4°C with anti-LRP1 antibody (1:500, Abcam, ab92544) in the same blocking solution. Cells were incubated with Alexa Fluor-conjugated secondary antibodies (1:500, Invitrogen, A32790) for 1 hour, washed with PBS (3 times, for 5 min each) and mounted on slides with Immu-Mount (#99904402, Thermo Fisher Scientific). Images were acquired with a Zeiss LSM 780 confocal microscope with a 63x objective and appropriate excitation wavelengths and emission filters. Laser power and acquisition settings were kept constant between image acquisitions for different conditions. Images were analyzed with ZEN and ImageJ software. The images shown are representative of cells from three independent experiments.

Enzyme-linked binding assay

RAW264.7 cells were cultured in a 96-well microplate at a density of 10^5 cells/ml. Cells were incubated for 1 h at 4°C with concentrations of recombinant TAFA-Fc or Fc proteins ranging from 0.74 nM to 500 nM, in PBS supplemented with 10% FCS. Cells were then washed with PBS, fixed by incubation with 4% paraformaldehyde (PFA) in PBS for 20 minutes and then incubated for 1 h at room temperature with goat anti-human Fc-HRP. The microplates were washed with PBS and peroxidase activity was measured by adding 100 μl/well 3,3‘,5,5‘-tetramethylbenzidine (TMB) and 30% hydrogen peroxide (Sigma-Aldrich) and incubating for 30 minutes at room temperature. Optical density was measured at 450 nm on a TriStar^2 S LB 942, Multimode Microplate Reader (BertholdTech). Results were analyzed with MikroWin software.

Slice preparation and treatment for electrophysiological recordings

The experiments were performed with WT mice (Charles River) for the recording of unidentified neurons or with the glutamic acid decarboxylase–green fluorescence protein (GAD67-GFP) knock-in mouse produced by Tamakaki, for recordings of $GAD67^-GFP^+$ or $GAD67^-GFP^-$ neurons. In both cases, recordings were performed in the lumbar spinal cord LIIi and LIIo. Adult WT and $GAD-67^{-GFP/+}$ mice (5 to 6 weeks old) were either used in naive conditions or after being subjected to SNI, as described above. We chose

to study this neuropathic pain model because the DH ipsilateral to the lesion presents a dense accumulation of activated microglia (that can be used as a landmark), mostly in the L3-L5 segments (47).

Mice were anesthetized by an injection of 100 mg/kg ketamine plus 10 mg/kg xylazine. They were then perfused via the left ventricle with solution 1, pH 7.4, 0–2°C, through which O_2 was bubbled, (Table S1). The lumbar region of the spinal cord was extracted, embedded in low-melting agarose and the L3 to L5 lumbar segments were then cut into 300 μm-thick coronal slices on a microtome (Leica VT1200, Leica Microsystems SAS). These steps were performed as quickly as possible. The slices were kept at least for 1 hour in solution 2 at 30°C (pH 7.4, 29°C, through which 95% CO_2-5% O_2 was bubbled; Table S1).

Slices obtained from mice subjected to SNI were incubated for 30 minutes in solution 2 to which Alexa Fluor 568-conjugated isolectin B4 (IB4; Invitrogen) was added, immediately before transfer to the recording chamber (see below) at room temperature. The IB4 labeling of activated living microglia (38) identified the area of the DHSC receiving the damaged primary afferent fibers and, thus, the site at which LIIi and LIIo neurons should be targeted for recordings. When necessary, we added 40 nM TAFA4 with or without 40 nM RAP to the IB4-containing solution 2 and, and the slices were incubated in this solution for 1 hour before recording.

Patch-clamp recordings

The borosilicate glass pipettes used had a resistance of 2.5 to 4 MΩ. Their tips were fire-polished with a Narishige microforge and coated with beeswax to reduce their capacitance. They were filled with the following intracellular solution: 125 mM potassium glutamate, 24 mM KCl, 1 mM EGTA, 10 mM HEPES, 0.1 mM $CaCl_2$, 2.5 mM $MgCl_2$, 0.3 mM GTP-Na, 2 mM ATP-Na_2).

The slices, immobilized with a nylon grid in an immersion-type recording chamber placed on the stage of an upright microscope (Olympus BX51WI, Olympus Fr., Rungis, France), were superfused at a flow rate of 2 ml/min with ACSF (solution 3, pH 7.4, room temperature, through which 95% CO_2-5% O_2 was bubbled; Table S1). In these conditions, the patch pipettes were guided to the neuron cell bodies, in the LIIo and LIIi lamina, with the aid of differential interface contrast optics with infrared illumination (X40, Olympus BX51) and fluorescence optics. The location of the neuron was captured by taking photographs with a camera (VX55 TILL Photonics). The recording sessions were performed after solution 3 had been replaced with modified ACSF (solution 4; Table S1) containing tetrodotoxin (TTX, 0.5×10^{-6} M; Bio-Teche (UK)) to block Na^+ currents and tetraethylammonium chloride (TEA-Cl; 36 mM) to block TEA-sensitive non-inactivating K^+ currents. Kv4 channels are the only Kv channels carrying I_A preserved at this high concentration of TAE-Cl (39). In a small set of experiments, we added 2 mM CsCl to solution 4, to block hyperpolarization-activated depolarizing currents (I_h), and 20 μM CdCl, to block Ca currents (I_{Ca}) other that T- type I_{Ca} currents, which are known to interact with the I_A carried by Kv4 channels (48, 49). I_A was then isolated by exploiting its sensitivity to holding potential: from a hyperpolarized membrane potential (−120 mV), depolarizing voltage steps evoked both transient and sustained K^+ current (total I_K), whereas, from a more depolarized membrane potential (−30 mV), depolarizing steps evoked only sustained K^+ currents (I_{KDR}; See protocol in Figures 4A and 5A). The conditioning prepulses at −120 or −30 mV lasted 750 ms and were immediately followed by 1 s depolarizing steps. I_A was revealed by the offline subtraction of I_{KDR} from total I_K.

For the hyperpolarized prepulse, we chose a highly hyperpolarized value (−120 mV) because, in our preliminary exploration of I_A in the dorsal spinal cord, we found that some neurons had a very hyperpolarized inactivation midpoint. This hyperpolarized prepulse also made it possible to detect and measure I_h. For this purpose, the holding current was subtracted for the comparison of I_h amplitude despite the presence of cell-to-cell variations in holding current values.

In the course of our preliminary exploration, we observed that it was difficult to maintain a stable series resistance over long recordings in five- to six-week-old mice. This made it impossible to obtain reliable results for the two successive, relatively long protocols required to obtain incremented difference current values from −70 mV to +100 mV for the construction of activation curves. We thus simply used test pulses to +70 mV from a holding potential of −120 or −30 mV (see protocol in Figures 4A and 5A). These suprathreshold values were chosen because, in the case of the LIIi-InhIN, I_A could be accurately measured only at such strongly depolarized potentials (see results); comparability was ensured by also applying these values for the other interneuron types.

Data acquisition and analysis

Patch pipettes were connected to the head stage of an Axopatch 200B amplifier. A computer interfaced to a 12-bit A/D converter (Digidata 1322A using pClamp10 (all from Molecular Devices, Sunnyvale, USA) controlled the voltage-clamp protocols and data acquisition. Data were digitized at 20 kHz and filtered at 2 kHz. Series resistances, without compensation, to ensure rapid recording, ranged from 6 to 19 MΩ (recordings with Ra > 19 MΩ were excluded). The mean liquid junction potential between the pipette solution and extracellular solution 4 was 12 mV, and was not corrected for.

Analyses and curve fitting were conducted in Clampfit 10.3 (Molecular Devices) and SigmaPlot 12 (Systat Software Inc. San Jose, CA).

I_h activation (Ihτ) was fitted for the traces obtained when stepping from −70 to −120 mV and was described as the sum of two exponential terms plus a constant according to the equation $Ih(\tau) = A_{fast} \exp(-t/\tau_{fast}) + A_{slow} \exp(-t/\tau_{slow}) + C$, where A_{fast} and A_{slow} are the amplitudes of the exponential terms and τ_{fast} and τ_{slow} are the corresponding time constants (τ). The weighted τ (τ_{wact}) was calculated as follows: $\tau_{wact} = (A_{fast} \times \tau_{fast} + A_{slow} \times \tau_{slow})/(A_{fast} + A_{slow})$.

Reverse transcription- quantitative polymerase chain reaction: RT-qPCR

Ipsilateral and contralateral L3, L4 and L5 DRGs and DHSCs (lumbar segments L3-L5) were dissected from P35 WT mice on day 7 post-SNI. RNA was extracted with the RNeasy Mini Kit (QIAGEN), in accordance with the manufacturer's instructions. RNA quality was controlled with the RNA Agilent Pico 600 kit (Agilent). We subjected 100 to 150 ng high-quality RNA (RIN > 9) to reverse transcription to generate cDNA (Superscript III, Thermo Fisher Scientific), which was then used as a template for quantitative PCR. Gene expression was quantified by qPCR in Sybr-Green master mix (Thermo Fisher Scientific). The relative abundances of the transcripts encoded by each gene were determined by normalization against β-actin by the standard ΔCt or ΔΔCt method.

The primers used for qPCR were:

TAFA4-Fw: CAGTTACAAAGGGACATTCACG
TAFA4-Rse: AGCACAGACTCTCATCCTTGG
LRP1-Fw: GGTGAAAGAGATTGCCCCGA
LRP1-Rse: CCCCAGACAACTGTGCTCAT
ATF3 Fw: GCTGGAGTCAGTTACCGTCAA
ATF3 Rse: CGCCTCCTTTTCCTCTCAT
Knca4 Fw: CACCCCCAATGATTCTGC
Knca4 Rse: TTCACAAGAAGCACTTCACCA
Kcnc1 Fw: ACTCAGAGTGACACATGCCC
Kcnc1 Rse: GCCACCTCCCCATTCAGTTT
Kcnc3 Fw: TATCCCCCTAGTGGACGAGC
Kcnc3 Rse: CCACAATGCTGCTCAGGCT
Kcnc4 Fw: CTCAGTGCTGGGGACTATGC
Kcnc4 Rse: GGCATAGTTGGACGAGAGGG
Kcnd1 Fw: GCACGAGCAAGACCAACTTC
Kcnd1 Rse: GCCTGCAATGGTGCTAGGTA
Kcnd2 Fw: ACCAACGAGCAGACAAACGA
Kcnd2 Rse: TTGCTCAGTAGCCCATTCCG
Kcnd3 Fw: TGCATCTTTCTGGTACACCATAGT
Kcnd3 Rse: GCTAAAGTTGGAGACTATCACAGG
Hcn1 Fw: GCCAGAGCACTTCGTATCGT
Hcn1 Rse: CACTGGCGAGGTCATAGGTC
Hcn2 Fw: ATGCTGCAAGACTTCCCCAG
Hcn2 Rse: GAAGAGCGCGAACGAGTAGA
Hcn3 Fw: AAGATCCTTAGCCTGCTGCG
Hcn3 Rse: GAAGATGCGAACCACTGCAC
Rse: GAAGATGCGAACCACTGCAC
Hcn4 Fw: CTCCCTAAGGATGTTCGGCA
Hcn4 Rse: CAGCAACAGCATCGTCAGGT

QUANTIFICATION AND STATISTICAL ANALYSIS

The results are expressed as means ± SEM. Statistical analyses were performed with Prism 7 (Graphpad Software, La Jolla, CA, USA). The significance of differences was assessed in multiple t tests against BSA for behavioral experiments and in unpaired t tests for electrophysiology experiments.